

Chapter-4

Provenance of sediments deposited in the Andaman Region

4.1 Introduction

Sediments are either produced by surface processes like weathering and erosion or by (bio) chemical precipitation. Deposited on dry lands and within bodies of water, sediments, store valuable information about processes that occur on the surface of the Earth. In fact, sedimentary records are the main source of our knowledge about tectonics, palaeoclimate, palaeogeography and evolution of life on our planet. Determining the provenance of sediments deposited in a basin is one of the most important aspects of studying sedimentary rocks. In geology, finding out provenance is not only restricted to deciphering lithologic origin of sediments but also involves reconstruction of their parent rock compositions, depositional history, and tectono-climatic conditions during their deposition. It has been realized that making inferences about sedimentary provenances is not simple. It requires detailed understanding of nature and extent of compositional and textural modifications suffered by sediments during weathering, erosion, deposition and diagenesis. To avoid any bias resulting from over-dependence on a single method, use of multiple proxies is preferred. Over the years, several techniques such as petrography, mineralogy of heavy and clay minerals and elemental and isotope geochemistry have been successfully developed and utilized in such studies (Thurach, 1884; Mackie, 1899; Krumbein and Pettijohn, 1938; Weltje and Eynatten, 2004 and references therein; Taylor and McLennan, 1985; Bhatia, 1983; Bhatia and Crook, 1986; Roser and Korsch, 1986).

In this work, we have used geochemical and isotopic tracers to determine provenances, understand tectonic settings and climatic conditions during the deposition of sediments in the forearc (accretionary prism) and backarc (Andaman Sea) basins of the Andaman Subduction Zone. The sedimentary sequences of the Andaman forearc basin are believed to have started depositing during the Paleocene and therefore, likely to have preserved

records of major geological events on and around Indian Plate since then. Information on the provenances and tectono-geomorphic conditions during the deposition of the sediments that make up the sedimentary rocks of the Andaman Islands is meagre. Therefore, a comprehensive geological, isotopic and geochemical study of these rocks is required to settle much of the outstanding issues related to the regional geology, stratigraphy, major tectonic changes and evolution of these islands.

The sedimentary record of the Andaman Sea, which came into existence during late Miocene or early Pliocene, provides another time window to study the provenances of sediments contributed to this region of South-East Asia and understand their transport dynamics and variations with changing climate and tectonics. Although at present, the basin largely receives sediments from the Irrawaddy, Salween, and Sittang Rivers of Myanmar (Rodolfo, 1969), it is yet to be established if the scenario were similar in the past. To answer this question and to understand the evolution of the basin as a whole, a comprehensive study of sedimentary record was deemed necessary.

Prior to the final collision of the Greater India with southern margin of the Eurasia in the north and ancient Myanmar in the east, the Sunda Arc extended well up to Pakistan as the Jurassic–Paleogene Trans-Himalayan Arc and suture zone (Mitchell, 1993). It is believed that this arc and suture zone formed an ancient Andean type margin along the Neo-Tethys (Chu et al., 2006; Scharer and Allegre, 1984) and marked the boundary between the Eurasian plate and the Indian plate (Clift et al., 2001; Sinclair and Jaffey, 2001). The final collision of these two plates occurred at ~50 Ma (Rowley, 1996; Hodges, 2000) and subsequently the Neo-Tethys started closing. Most of the authors propose that the Himalayan thrust belt started developing on the Indian plate margin as a result of continent-continent collision during the Neogene (e.g., Johnson and Alam, 1991; Rahman and Faupl, 2003; Uddin and Lundberg, 1998), while the eastern sector (Myanmar) of the subduction zone continued to remain active. A trench-forearc basin opened up along the subduction trench, on the east of the Indian plate margin, while on the Indian plate two

remnant ocean basins, Katawaz and Bengal, remained active (Alam et al., 2003; Qayyum et al., 2001).

Sedimentary records of the suture zone show that until ~55 Ma the Trans-Himalayan landmass was the predominant source of sediments, while the Greater Indian landmass contributed only subordinately to the basins in the north (Garzanti and Vanhaver, 1988; Wu et al., 2007; Sinclair and Jaffey, 2001). The foreland and Bengal basins lying south of the Himalaya observed multiple changes in provenances of sediments they received during the late Paleocene to mid Eocene, however, only one such change has been reported at the beginning of the Oligocene (Najman et al., 2008). It has been shown by Najman et al. (2008) that the major changes in sediment provenance in the Bengal basin (from ~38 Ma during the deposition >1 km thick sand beds of the Barail Group) are related to the increase in contribution from the thrust and uplifted Indian crust along the nascent Himalayan mountain belt. Another study by Lindsay et al. (1991) also reported large scale deposition of materials derived from the Himalaya in the northern Bengal basin at ~40 Ma. Such changes have also been observed in the Andaman Islands during the Oligocene (Pal et al., 2003; Allen et al. 2007). This synchronous change in provenance across the basins south of the Himalaya hint at occurrence of a major tectonic (thrusting) event in the Himalaya during this time. Another such major geological event, evident from regional upliftment and stratigraphic changes in the Irrawaddy delta, Mergui Basin, and in the Indo-Burman Ranges, has been reported at ~20 Ma (Acharyya et al., 1989).

4.2 Potential source for Andaman forearc and backarc deposits

In order to characterize the provenances of sediments deposited within the Andaman forearc and backarc basins it is essential to first locate and understand potential sources. In this section we identify four such source regions and describe their chemical characteristics. Table 4.1 lists these sources and their important features. The potential sources identified for both the forearc and backarc basin deposits are: Suprasubduction and Arc magmatic rocks, rocks from the Himalayan-Trans-Himalayan region, rocks of the Indian Shield and Myanmar. Figure 4.1 shows most probable paleogeographic

configuration of various tectonic blocks in south Asia prior to the closure of Neo-Tethys. These blocks contain the potential sources of sediments deposited in the Andaman forearc basin during the Paleogene.

4.2.1 *Suprasubduction and Arc igneous sources*

These include the suprasubduction ophiolite and magmatic arc rocks of the region. Such sources were present all along the Sunda Arc in the south to the Himalayan Arc and suture zone in the north (Fig. 4.1). As discussed in earlier chapters the ophiolite sequence from the Andaman consists of mantle rocks, plagiogranites, mafic plutonic and intrusives, and extrusive lava series- most of which have been altered. The magmatic arc sources from the region have mafic, intermediate and felsic volcanic products (Chhibber, 1934, Mitchell, 1985; Wakita, 2000; Hall 2002, 2009; Van Bemmelen, 1949). The only isotopic study on the ophiolites of the Andaman Islands (Kumar, 2011) reveals that their $^{87}\text{Sr}/^{86}\text{Sr}$ ratio varies between 0.70342 and 0.70483, whereas ϵ_{Nd} varies between +6.4 and +11.7. The ophiolitic and early magmatic arc sources would have become important during the initial trench and forearc basin fillings, whereas the recent volcanism (<4 Ma) would have acted as sources to the back arc fillings.

4.2.2 *Indian Shield Sources*

The Indian shield lying west of the Andaman Basin was made up of 5 cratons- Aravalli, Bundelkhand, Singhum, Bastar and Dharwar joined by mobile belts (Fig. 4.1). These mostly consisted of Archean gneisses, granites and schists and Proterozoic sedimentary successions. Materials derived from these cratons would have been predominantly arkosic with minerals reflecting old continental crust of Precambrian–Late Palaeozoic age (Najman et al., 2008; Misra and Johnson, 2005; Auge et al., 2003; Mishra et al., 1999). ϵ_{Nd} of materials derived from Archean rocks should have been ≤ -30 (Najman et al., 2008; Peucat et al., 1989; Saha et al., 2004). Considering the paleogeographic positions of various cratons and major drainage patterns during the Paleogene, we believe that the parts of the Indian shield that would have contributed sediments to the Andaman trench-forearc basin were the Proterozoic Chotanagpur and Shillong Plateaus (Fig. 4.1).

Table 4.1: Summary of salient features of potential source regions for Andaman Sediments

Source Regions	Lithology	U-Pb zircon ages (Ma)	Ar-Ar mica ages (Ma)	$^{87}\text{Sr}/^{86}\text{Sr}$	$\epsilon_{\text{Nd}}(t)$
<u>Igneous Sources</u>					
Andaman and Indo-Burman	Suprasubduction ophiolites Magmatic arc volcanics	Late Cretaceous (93.6±1.6 Ma, 95±2 Ma)		0.7034-0.7048	+6.5 to +11.8
<u>Himalaya</u>					
Higher Himalaya	Quartzofelspathic, Med-high grade metamorphic rocks	Cambro-Ordovician to Archean (>3000 Ma. Pks: 1100, 1500-1700, 2500)	Tertiary (dominant)	0.7331-0.9062	-20 to -5
Tethyan Himalaya & Haimanta Group	Sedimentary & low grade metamorphic rocks	Cambro-Ordovician to Archean (500 to >3000 Ma Pks: 500, 1100, 2500)	Pre-Tertiary; <950 Ma, mostly <500 Ma (from Cambro-Ord granites)	0.7158-1.1764	-30 to -16
Arc & Suture Zone	Batholiths (Gangdese & Nyainqentanglha), Ophiolites	Jurassic-Eocene (<200 Ma, Numerous peaks: 50, 80-90, 150, 200 Ma)	Cretaceous and Tertiary		+1 to +8
<u>Indian Shield</u>					
Chotanagpur Proterozoic gneissic belt (river sand data)	Gondwanan seds. Gneiss. Granites. Arkosic sediments	Proterozoic (950-1450, pk: 1350-1400 Ma)	Proterozoic (788-938 Ma)	0.7625-0.9724	-13.8
Shillong Plateau (river sand data)	Precambrian-Late Palaeozoic gneiss & granite	Proterozoic & Cambro-Ordovician (500-1800 Ma)	Cambro-Ordovician (467-524 Ma)	≥0.735	-14.6
<u>Myanmar</u>					
Shan-Thai block	Proterozoic-Cretaceous sedimentary rocks on schist basement. Cretaceous arc rocks, Mogok schists, gneisses and intrusives	Tertiary aged zircons along the Burma margin I-type granitoids ages: 120-150 Ma	Mica ages along Shan Scarp: 26-16 Ma K-Ar mineral dating of batholiths: 79-100 Ma		

Data sources: Allen et al., (2007); Allen et al., (2008); Najman et al., (2008); Singh and Krishna, (2009); Zhao et al., (2009); Pederson et al., (2010); Sarma et al., (2010) and Ullah, (2010);.

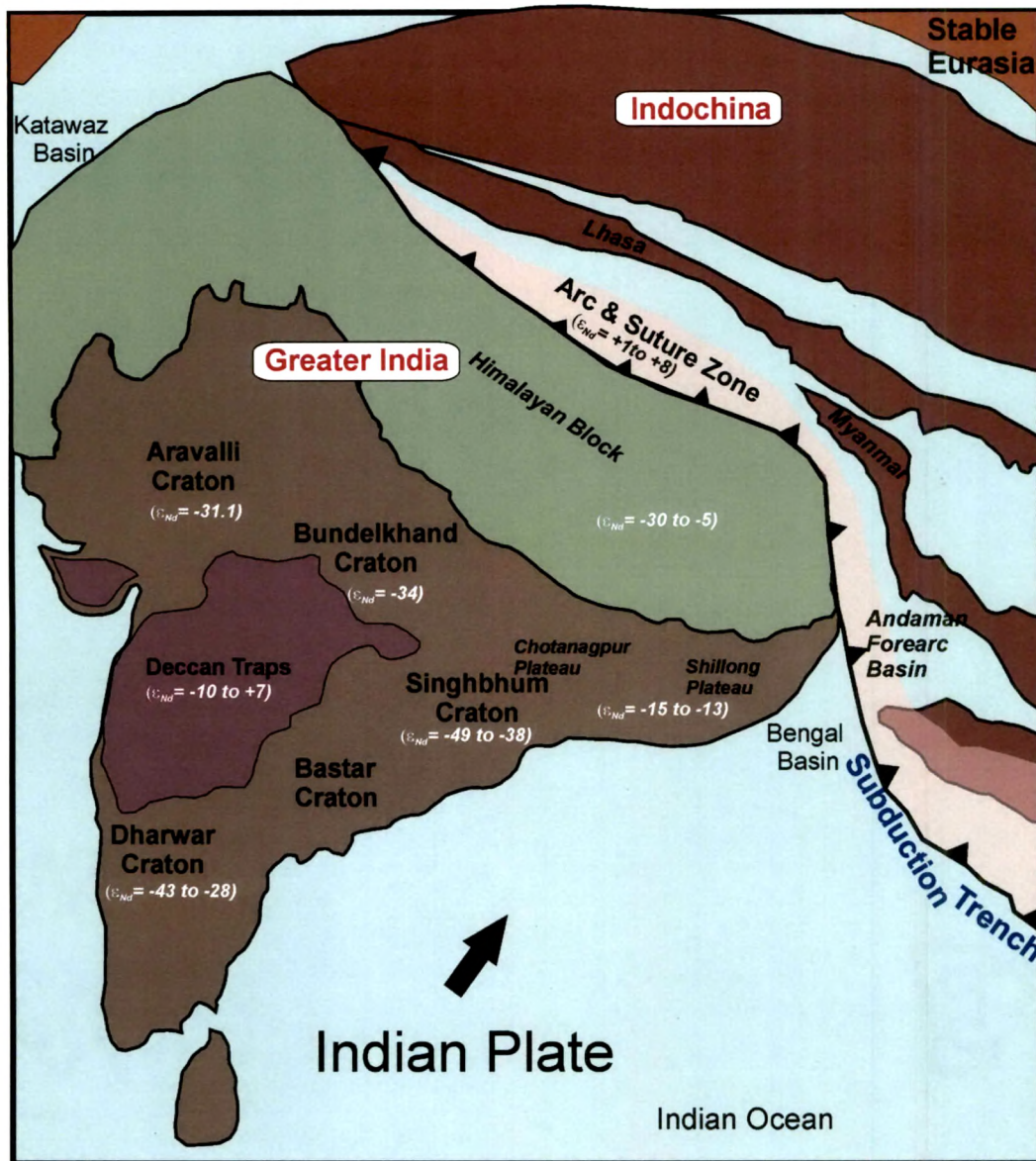


Fig. 4.1: Schematic map (modified after Replumaz and Tapponnier, 2003) showing the potential source regions for sediments deposited in the Andaman forearc basin during the Paleogene. Data sources: Sharma et al. (1994); Jayananda et al. (2000); Allen et al. (2007); Allen et al. (2008); Najman et al. (2008); Sheth et al. (2009b); Singh and Krishna (2009); Zhao et al. (2009); Ullah (2010) and Shukla (2011).

The sediments carried by rivers draining through these areas deposited detrital zircons and micas having (fission track and Ar–Ar) ages older than 467 Ma, with ϵ_{Nd} values varying from -15 to -13 (Table 4.1, Najman et al., 2008).

4.2.3 Himalayan and Trans-Himalayan Sources

The rocks that today occupy the trans, higher and lesser Himalayas were part of either the greater Indian plate or the sediments deposited in Neo-Tethys. Going by the present day configuration one would expect that the potential sources of the forearc sediments were mainly consisted of rocks of the Jurassic–earliest Tertiary batholiths of the Trans-Himalaya (Scharer and Allegre, 1984), the south-directed thrust belts of ophiolites and Palaeozoic–earliest Tertiary Tethyan sediments (DeCelles et al., 2001; Maheo et al., 2004). The Higher Himalayan sources would have included Oligocene-Miocene metamorphic rocks (Hodges, 2000; Vance and Harris, 1999) and those in the Lesser Himalayan were Precambrian to Cretaceous age, weakly to non-metamorphosed rocks of the Indian plate (Hodges, 2000; Richards et al., 2005). The ϵ_{Nd} data from the Trans-Himalayan Arc and suture zone sources today vary from +1 to +8 (Clift et al. 2001; Maheo et al. 2004), while the Higher and Lesser Himalayan sources have values varying from -30 and -5 (Ahmad et al., 2000; Robinson et al., 2001; Richards et al., 2005, Zhao et al., 2009).

4.2.4 Myanmar Sources

The Burmese margin to the east of the Andaman forearc basin was characterised by the older Cretaceous Mogok Metamorphic belt during the Paleogene. This belt continued north-west as the Trans-Himalayan (*Gangdese Batholith, Lhasa and Karakoram Terranes*) ancient active margin of Asia (Barley et al., 2003; Mitchell, 1993) (Fig. 4.1). In Myanmar, the active margin was represented by the Tertiary volcanic belt containing the now-extinct volcano- Mt. Popa (Stephenson and Marshall, 1984). The tectonic belt to the east, continued south up to Thailand and exposed rocks of Carboniferous to Permian age (Garson et al., 1976) that were intruded by tin-tungsten bearing granite plutons of Paleocene age having $^{87}Sr/^{86}Sr$ ratio ≥ 0.717 (Mitchell, 1985).

4.3 Provenance of sediments of the Andaman Islands

4.3.1 Background and Earlier work

Of the five groups of sedimentary rocks of the Andaman and Nicobar Islands, the lithostratigraphy of only two, the late Paleocene-Eocene Mithakhari and the Oligocene

Andaman Flysch, are dominated by siliciclastic sediments and therefore, we focused our study of provenances on them. The nature of provenance for the sediments of the Andaman forearc, particularly the Andaman Flysch Group, has remained controversial. Many earlier workers (e.g. Karunakaran et al., 1968a and Pal et al., 2003) believed that Irrawaddy sediments were the main source for the Andaman Flysch Group rocks, whereas others (e.g., Moore et al., 1982 and Curray et al., 1979, 2005) believed that these sediments were originally derived from the emerging Himalayas and were transported by the rivers draining into the Bengal Fan. It is, however, not clear from these studies that whether these sediments were deposited directly in the forearc or got offscraped from the subducting Indian slab at a later time. Other sources, which were thought to have contributed sediments to the Andaman forearc, were the northward-drifting greater Indian shield and eastern Myanmar (Allen et al., 2007).

In a recent work, Allen et al. (2007) made attempts to determine provenances of sediments that form the Andaman accretionary prism. Based on petrographic, isotopic ($^{143}\text{Nd}/^{144}\text{Nd}$ of apatites) and mineral (apatite and zircon) cooling ages they proposed that the sediments of the Mithakhari Group were predominantly derived from the nearby arc sources, with subordinate contributions from an older continental source containing sedimentary and low-grade metasedimentary rocks- most likely located on the northeastern region of Myanmar. They also proposed that the sediments of the Andaman Flysch Group were derived from “recycled orogenic” sources consisting of very low to high rank metapelite-metapsammite sediments and a subordinate arc source. In the absence of appropriate geochemical and/or isotopic data from the sources located in Myanmar, discrimination between Himalayan-Transhimalayan and Myanmar sources was not possible and hence, the authors could not rule out completely the contributions from the Himalayan-Transhimalayan sources to the Andaman forearc sediments. U-Pb ages of detrital zircons and Ar-Ar ages of detrital white micas from Andaman sediments also suggest contributions from older continental crust as well as younger arc sources (Allen et al., 2007). The Ar-Ar ages of detrital micas from the Mithakhari Group fall between the Paleozoic to Mesozoic, whereas those from the Andaman Flysch fall mainly between Late

Mesozoic and Tertiary. The U-Pb detrital zircon ages from the Andaman Flysch span from 100 to 1500 Ma, with two strong modes in Proterozoic and Cretaceous–Eocene. From mineralogical studies, plagioclase, quartz, K-feldspar, pyroxene, epidote, sphene, green-brown hornblende, chromian spinel, apatite, garnet, rutile, and titanium oxides have been reported from the Mithakhari Group while quartz, K-feldspar, plagioclase along with zircon, tourmaline, rutile, and chromian spinel have been reported from the Andaman Flysch Group. From these studies it appears that Andaman sediments contain very little, if any, material from the cratons in the Indian shield, however, many contain materials derived from the Proterozoic sedimentary sequences of the Greater India including those presently located within the Himalayan mountain belt.

4.3.2 Results of our study

(A) Petrography

Petrographic study on sedimentary rock samples from various formations of the Andaman sequences reveals that these formations have not undergone metamorphism. Important textural and mineralogical characteristics of the formations are described below.

1) Mithakhari Group

a) Hopetown Conglomerate

The Hopetown conglomerate near Chidiyatapu primarily contains feldspars with subordinate quartz, lithic grains and fossils, mainly foraminifers (Fig. 4.2a & b).

b) Namunagarh Grit

The Namunagarh Grit unit, extensively present as coarse grained sandstones, contains quartz, plagioclase and lithic fragments. Both monocrystalline and polycrystalline varieties of quartz have been observed. Fractures are common within these quartz crystals that probably reflect the effect of tectonics (Fig. 4.2c). We observe pumice fragments, glass shards and grains of plagioclase and pyroxene cemented in a siliceous matrix (Fig. 4.2d). The presence of angular mineral grains suggests short distance transportation.

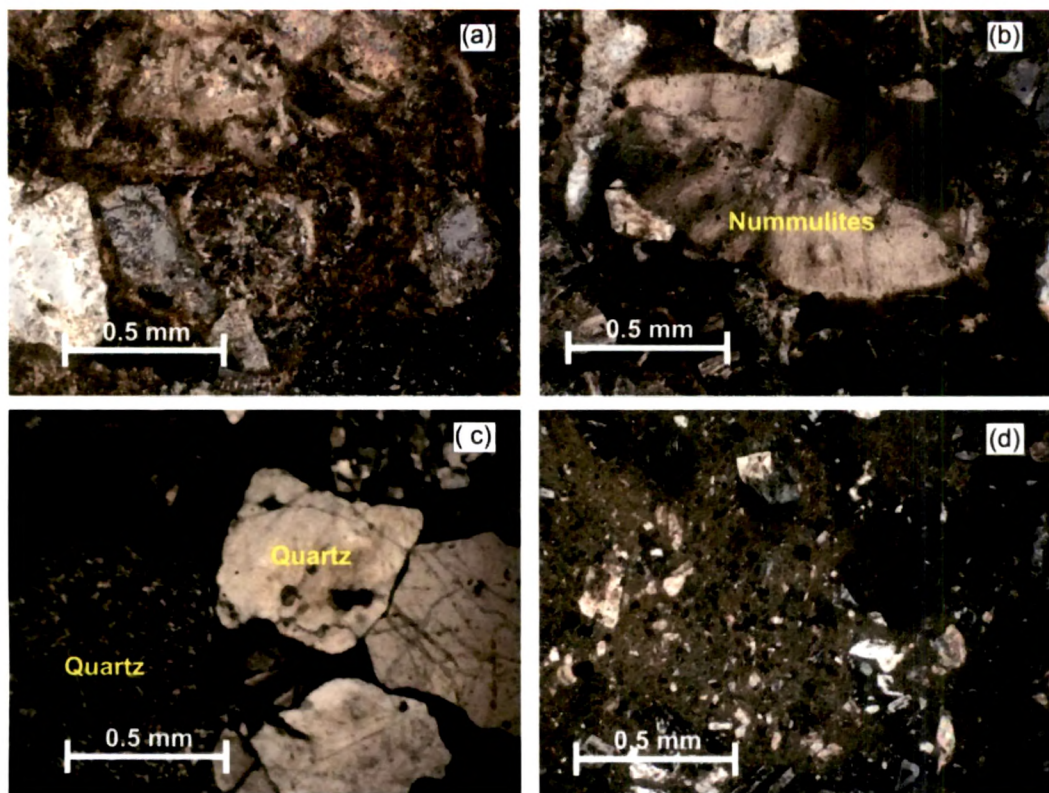


Fig. 4.2: Photomicrographs of thin sections: (a) & (b) Hopetown conglomerate unit of the Mithakhari Group showing shells of foraminifers (Nummulites) in coarse gritty matrix (c) Namunagarh grit unit of the Mithakhari Group (d) Tuff in the Mithakhari Group, Middle Andaman.

2) Andaman Flysch Group

The sandstone and shale formations of the Andaman Flysch Group are made up of quartz, feldspars and clay minerals (Fig. 4.3b). In comparison to the Mithakhari Group rocks, these are much finer in grain size and contain more quartz. Accessory minerals include zircon, tourmaline, rutile and spinel.

3) Archipelago Group

The limestone formations of the Archipelago Group are fossiliferous and contain shells of cephalopods, gastropods and foraminifers. They also contain sand grains and lithic fragments of volcanic origin. Figures 4.3c & d show photomicrographs of thin sections of two such formations.

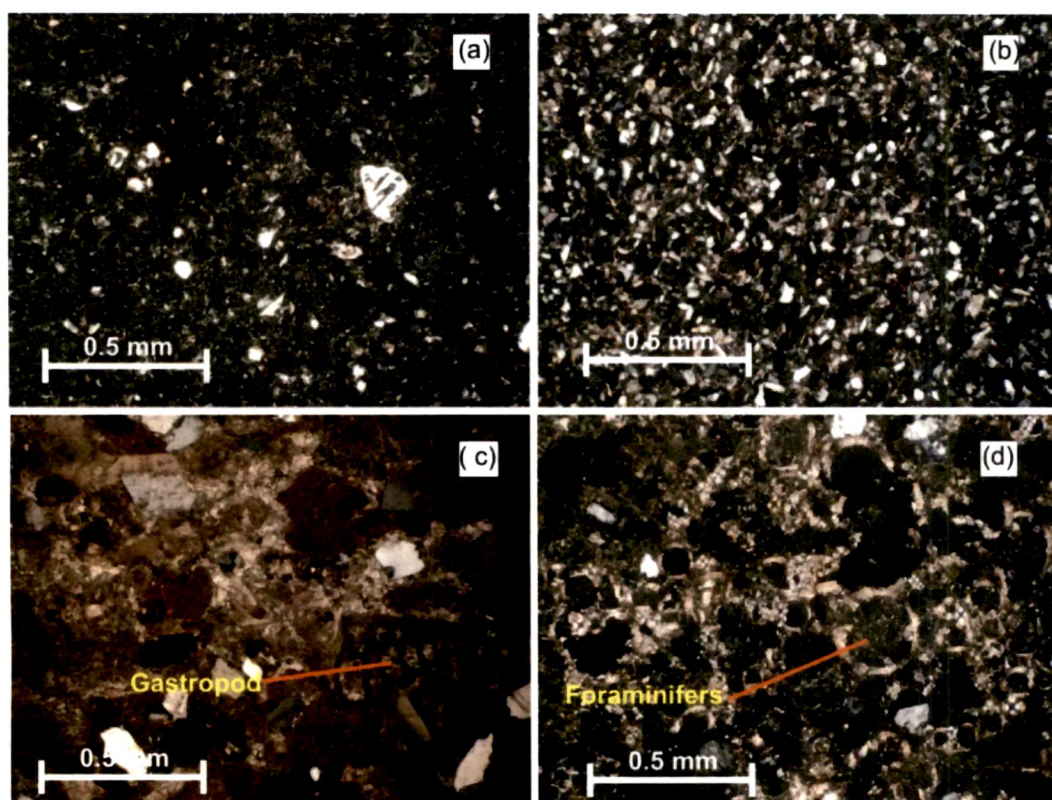


Fig. 4.3: Photomicrographs of thin section showings: (a) Grains of quartz in a fine grained matrix from turbidites of Kalipur (b) Shale of Andaman Flysch Group (c) Baratang Cave limestone showing shell of gastropod along with fragments of quartz and feldspar (d) Foraminiferal limestone of Archipelago Group from Havelock Island.

(B) Elemental Geochemistry

Concentrations of major and trace elements, including rare earth elements (REE), in the samples from the siliciclastic formations of the Mithakhari and Andaman Flysch Groups, are presented in Tables 4.2, 4.3 and 4.4. The Chemical Index of Alteration (CIA) (Nesbitt et al., 1996) for each sample, as presented in the Table 4.2, is calculated using molecular proportions of oxides as follows:

$$\text{CIA} = [\text{Al}_2\text{O}_3 / (\text{Al}_2\text{O}_3 + \text{K}_2\text{O} + \text{Na}_2\text{O} + \text{CaO}^*)] 100$$

where CaO* represents CaO contents of silicate minerals only. Figure 4.4 shows variations of the major element oxide versus SiO₂ contents in all our samples. Trace element contents, isotopic compositions (⁸⁷Sr/⁸⁶Sr and ε_{Nd}) and Nd-model ages (T_{DM}) for these samples are

presented in Tables 4.3 (Mithakhari Group) and 4.4 (Andaman Flysch Group). Figure 4.5 shows primitive mantle-normalized trace element patterns (a & b) and chondrite-normalized REE patterns of these samples (c & d). From the geochemical data we make following observations.

1. The rocks of the Mithakhari Group are characterized by lower SiO_2 contents, lower $\text{K}_2\text{O}/\text{Na}_2\text{O}$ and intermediate to higher $\text{Fe}_2\text{O}_3^{\text{T}}$ and MgO contents in comparison to the rocks of the Andaman Flysch Group and Post-Archean Australian Shale (PAAS) (Fig. 4.4).
2. The CaO content in these rocks are much higher than that in the Andaman Flysch rocks (Fig. 4.4d). Considering that these rocks do not contain much carbonates, we infer that high CaO is a result of high plagioclase content, which is supported by high Na_2O abundance in these rocks (Fig. 4.4f).
3. The Andaman Flysch sediments, apart from having higher SiO_2 , also contain higher amounts of Al_2O_3 and K_2O .
4. Sample AND-09-41, a siliceous limestone, is characterized by very low SiO_2 and high CaO content.
5. Unlike other Mithakhari formations, AND-09-48, a shale unit, has very high $\text{K}_2\text{O}/\text{Na}_2\text{O}$ ratio.
6. The primitive mantle-normalized trace element patterns for Andaman siliciclastics (Fig. 4.5a & b) are similar to PAAS, however, show more pronounced depletions in Ba, Nb, Ta, Sr, and P. The amounts of these depletions are much higher in rocks of the Mithakhari Group compared to those of the Andaman Flysch Group (Fig. 4.5a & b).
7. The contents of Large Ion Lithophile Elements (LILE) in the Andaman Flysch rocks are generally higher than that in the Mithakhari rocks and plot closer to the pattern of PAAS (Fig. 4.5b).
8. The trace element patterns of the Mithakhari rocks overlap with the field of the Andaman Ophiolites, whereas those of the Andaman Flysch rocks plot well within the field defined for the Himalaya (Fig. 4.5a & b).

Table 4.2: Major oxide compositions (in wt. %) for siliciclastic sedimentary rocks of the Mithakhari Group and Andaman Flysch Group of Andaman Islands

(wt. %)	SiO ₂	TiO ₂	Al ₂ O ₃	Fe ₂ O ₃ ^T	MnO	MgO	CaO	Na ₂ O	K ₂ O	P ₂ O ₅	LOI	K ₂ O/Na ₂ O CIA
<i>Mithakhari Group</i>												
AND-09-02	54.03	1.05	14.57	10.32	0.33	5.30	6.10	8.13		0.17	6.45	50.58
AND-09-03	67.39	0.82	14.99	6.58	0.10	3.62	2.47	2.72	1.19	0.12	3.60	70.75
AND-09-06	60.94	1.06	16.82	10.16	0.44	2.17	4.70	3.18	0.45	0.08	4.65	67.17
AND-09-09	70.53	0.61	12.32	9.80	0.10	2.68	2.26	1.15	0.33	0.22		77.04
AND-09-10	63.10	0.68	14.52	7.33	0.18	4.57	5.24	3.20	1.08	0.11	5.15	61.00
AND-09-11	69.09	0.49	13.02	3.43	0.24	3.36	7.46	1.52	1.31	0.10		56.39
AND-09-13	71.65	0.70	14.20	5.99	0.09	2.31	2.05	2.36	0.55	0.10		74.49
AND-09-15	50.43	0.63	13.74	5.98	0.12	5.77	17.31	5.48	0.43	0.11		37.22
AND-09-16	55.15	1.04	14.60	12.30	0.28	6.82	3.14	6.54		0.13		60.12
AND-09-18	59.43	0.88	15.34	6.66	0.24	2.06	12.99	1.46	0.84	0.09		50.37
AND-09-20	61.75	1.30	15.74	10.82	0.14	2.91	1.89	4.97	0.34	0.14	2.75	68.78
AND-09-23	63.22	1.26	16.59	10.26	0.09	3.31	3.25	1.43	0.37	0.22		76.94
AND-09-24	55.89	0.62	12.56	3.30	0.34	1.51	23.33	1.82	0.45	0.17	12.80	32.97
AND-09-27	73.53	0.60	14.94	5.34	0.02	2.48		1.13	1.92	0.05	3.95	84.08
AND-09-28	69.73	0.63	16.89	1.99	0.07	1.32	4.51	4.63	0.12	0.10		64.60
AND-09-30	62.07	1.10	13.74	10.77	0.15	4.67	3.25	3.47	0.61	0.17	3.25	65.58
AND-09-37	67.47	0.61	12.10	4.29	0.28	2.09	10.01	2.73	0.32	0.09	6.18	48.18
AND-09-41	33.43	0.26	3.06	2.40	0.80	1.93	36.01	0.00	0.16	0.28	31.84	7.81
AND-09-44	62.70	0.83	15.83	9.90	0.11	4.26	3.05	1.42	1.78	0.11	6.30	72.41
AND-09-48	64.58	1.09	16.07	10.41	0.30	1.96	2.51	0.51	2.47	0.10	5.90	76.59
AND-09-49	64.39	0.89	14.90	9.40	0.47	2.89		6.20	0.78	0.09	3.35	68.34
AND-09-51	75.16	0.72	11.95	6.89	0.08	2.50		2.60		0.11		82.15
AND-09-52	67.51	1.02	17.19	8.38	0.01	2.27		1.09	2.49	0.03		84.16
AND-09-55	64.11	0.75	14.05	8.84	0.13	4.17	1.79	5.59	0.43	0.13	2.45	64.41
PB-08-07	67.40	1.07	17.36	7.75	0.09	2.29		1.27	2.61	0.16		83.76
PB-08-08	67.66	0.97	16.19	6.76	0.06	3.35	0.28	2.54	2.06	0.14		78.13
PB-08-13	65.32	0.85	14.82	8.67	0.11	4.62	2.27	2.05	1.20	0.10	3.25	74.02
<i>Andaman Flysch Group</i>												
AND-09-04	65.90	0.92	16.88	7.35	0.18	2.55	1.89	2.00	2.18	0.14	4.19	74.25
AND-09-05	67.38	0.90	15.64	7.61	0.13	2.29	1.84	2.17	1.92	0.11		73.94
AND-09-12	74.11	0.93	15.82	4.15	0.04	1.50		0.94	2.41	0.11	1.90	84.42
AND-09-14	77.57	0.87	13.02	3.21	0.02	2.13		1.80	1.61	0.07	3.09	79.91
AND-09-36	68.30	0.58	17.57	6.22	0.05	2.30		2.01	2.51	0.16	3.05	81.28
AND-09-43	65.88	1.08	18.78	7.79	0.05	2.20		1.08	3.02	0.13	6.25	82.50
AND-09-61	67.59	1.15	24.50	1.11	0.01	1.40		0.72	3.48	0.05		86.64
PB-08-09	68.73	1.19	15.68	7.52	0.20	2.03	0.65	1.36	2.52	0.13		79.57

All values are normalized to 100% on a volatile free basis. LOI= Loss on Ignition

Table 4.3: Trace element concentration and isotopic ratio data for siliciclastic sedimentary rocks of the Mithakhari Group

	AND-09-02	AND-09-03	AND-09-06	AND-09-10	AND-09-19	AND-09-20	AND-09-22
(ppm)							
Rb	6.80	54.80	41.45	41.47	28.10	19.37	13.32
Sr	194.39	70.24	53.47	134.01	41.37	136.63	35.47
Ba	518.95	96.42	110.77	126.30	81.84	118.60	64.28
Y	79.63	9.01	13.83	12.23	15.23	18.85	19.33
Zr	64.80	16.37	24.20	24.12	23.94	61.40	60.61
Hf	2.20	1.07	1.21	1.22	1.52	2.30	2.16
Nb	2.35	5.98	3.43	3.46	3.85	3.83	3.51
Ta	0.21	0.53	0.26	0.26	0.25	0.24	0.22
Th	2.59	8.64	5.55	5.55	3.06	2.12	2.28
U	0.94	1.38	0.87	0.87	1.35	0.67	0.72
La	33.68	26.11	16.23	16.26	11.97	10.85	12.41
Ce	54.27	53.24	35.46	35.54	28.90	22.69	26.89
Pr	12.74	6.27	4.35	4.36	4.06	3.33	3.75
Nd	56.79	23.50	17.13	17.17	18.88	14.73	16.52
Sm	15.42	4.57	3.73	3.74	5.36	3.73	3.92
Eu	4.58	0.99	0.98	0.99	1.60	1.51	1.25
Gd	16.13	4.09	3.60	3.62	5.73	4.05	4.20
Tb	2.49	0.48	0.51	0.51	0.80	0.62	0.61
Dy	15.98	2.62	3.10	3.11	4.59	4.26	3.96
Ho	2.83	0.46	0.55	0.55	0.76	0.83	0.75
Er	8.18	1.35	1.56	1.57	2.04	2.55	2.24
Tm	1.01	0.17	0.20	0.20	0.25	0.34	0.29
Yb	6.72	1.14	1.36	1.37	1.65	2.37	2.02
Lu	0.97	0.16	0.19	0.19	0.23	0.35	0.30
Sc	24.87	5.44	8.60	6.07	10.21	16.09	14.79
V	167.16	44.86	49.58	41.61	80.78	55.11	98.61
Cr	17.24	71.72	10.90	103.87	121.76	-5.11	-3.74
Co	20.58	12.45	8.02	11.80	26.02	5.35	7.44
Ni	44.81	79.20	4.15	135.11	190.35	-1.57	10.00
Pb	9.27	13.21	12.30	12.31	8.12	7.36	14.30
Cs	0.20	3.36	2.85	2.85	1.85	0.73	0.89
Th/Sc	0.10	1.59	0.65	0.91	0.30	0.13	0.15
Zr/Sc	2.61	3.01	2.82	3.97	2.34	3.82	4.10
La/Th	13.03	3.02	2.92	2.93	3.91	5.12	5.45
Th/Yb	0.38	7.57	4.07	4.07	1.85	0.90	1.13
⁸⁷ Sr/ ⁸⁶ Sr	0.70657	0.71002	0.70665	0.70693	0.70800	0.70551	0.70683
¹⁴³ Nd/ ¹⁴⁴ Nd	0.512851	0.512344	0.512708	0.512502	0.512500	0.512835	0.512823
$\epsilon_{Nd}(0)$	4.2	-5.7	1.4	-2.7	-2.7	3.8	3.6
T_{DM} (Ga)	0.70	1.13	0.69	1.04	1.86	0.62	0.57

The trace elements concentrations are given in 'ppm'. Sr and Nd isotopes are given as ratios ⁸⁷Sr/⁸⁶Sr and ¹⁴³Nd/¹⁴⁴Nd. As variations in ¹⁴³Nd/¹⁴⁴Nd ratios are very less, to magnify the variation it is generally, represented by parameter ϵ_{Nd} . This parameter ϵ_{Nd} at present is defined by:

$$\epsilon_{Nd}(0) = \left\{ \left[\left(\frac{^{143}\text{Nd}}{^{144}\text{Nd}} \right)_s - \left(\frac{^{143}\text{Nd}}{^{144}\text{Nd}} \right)_{\text{CHUR}} \right] / \left(\frac{^{143}\text{Nd}}{^{144}\text{Nd}} \right)_{\text{CHUR}} \right\} \times 10^4$$

where subscripts 's' stands for sample and 'CHUR' stands for Chondrite Uniform Reservoir. The present day ¹⁴³Nd/¹⁴⁴Nd value of CHUR is 0.512638 (Depaolo and Wasserburg, 1976). In the results the parameter ϵ_{Nd} is taken for the present value of CHUR, so the subscript '(0)' has been omitted.

$$T_{DM} = 1/\lambda \left\{ 1 + \left[\left(\frac{^{143}\text{Nd}}{^{144}\text{Nd}} \right)_s - \left(\frac{^{143}\text{Nd}}{^{144}\text{Nd}} \right)_{DM} \right] / \left[\left(\frac{^{147}\text{Sm}}{^{144}\text{Nd}} \right)_s - \left(\frac{^{147}\text{Sm}}{^{144}\text{Nd}} \right)_{DM} \right] \right\}$$

where subscripts 'DM' stands for depleted mantle, $\left(\frac{^{143}\text{Nd}}{^{144}\text{Nd}} \right)_{DM} = 0.513114$ and $\left(\frac{^{147}\text{Sm}}{^{144}\text{Nd}} \right)_{DM} = 0.222$ (Michard et al., 1985).

Table 4.3: Continued

	AND-09-24	AND-09-27	AND-09-30	AND-09-37	AND-09-41	AND-09-44	AND-09-48
(ppm)							
Rb	27.00	89.24	25.03	22.05	13.42	76.62	92.89
Sr	127.25	36.59	153.85	101.54	552.49	56.08	92.03
Ba	55.14	83.36	417.42	70.54	142.26	114.97	147.88
Y	16.65	13.56	31.99	11.55	16.08	16.48	10.12
Zr	26.07	68.35	144.96	17.67	13.65	44.75	66.15
Hf	1.25	2.23	4.10	1.03	0.67	1.78	2.53
Nb	4.33	6.81	5.88	3.88	2.91	6.45	10.37
Ta	0.27	0.42	0.36	0.25	0.17	0.41	0.63
Th	3.32	7.12	5.06	3.08	1.16	5.85	6.44
U	0.73	2.21	1.32	0.67	0.16	1.28	1.27
La	19.10	22.98	17.45	14.68	21.06	19.43	18.08
Ce	36.99	43.70	39.38	30.17	22.71	43.82	46.79
Pr	4.60	4.86	5.37	3.82	4.57	5.55	5.40
Nd	18.54	17.34	23.15	15.42	18.31	22.93	22.02
Sm	4.20	3.24	5.74	3.44	3.65	5.30	4.91
Eu	1.21	0.64	1.53	0.99	0.93	1.32	1.17
Gd	4.57	3.05	6.11	3.60	3.98	5.27	4.62
Tb	0.63	0.39	0.92	0.51	0.54	0.72	0.62
Dy	3.97	2.61	6.14	2.98	3.39	4.23	3.62
Ho	0.72	0.51	1.19	0.50	0.63	0.74	0.62
Er	2.03	1.67	3.65	1.32	1.83	2.07	1.74
Tm	0.25	0.24	0.48	0.16	0.23	0.25	0.22
Yb	1.69	1.79	3.38	1.04	1.45	1.70	1.48
Lu	0.23	0.27	0.51	0.14	0.19	0.23	0.21
Sc	6.93	6.59	20.35	4.45	0.67	10.89	12.98
V	54.26	52.67	110.21	24.43	11.05	84.21	110.90
Cr	64.45	32.98	112.67	43.26	9.10	105.90	55.11
Co	8.33	7.02	14.13	6.26	2.05	15.41	21.28
Ni	45.72	35.78	104.93	44.50	30.65	160.35	69.67
Pb	10.37	14.35	10.52	8.03	18.73	11.58	16.14
Cs	1.32	5.31	3.41	1.04	0.57	5.87	5.70
Th/Sc	0.48	1.08	0.25	0.69	1.72	0.54	0.50
Zr/Sc	3.76	10.37	7.12	3.97	20.24	4.11	5.10
La/Th	5.76	3.23	3.45	4.77	18.12	3.32	2.81
Th/Yb	1.96	3.97	1.50	2.95	0.80	3.43	4.35
$^{87}\text{Sr}/^{86}\text{Sr}$	0.70749	0.71196	0.70576	0.70703	0.70732	0.70952	0.71021
$^{143}\text{Nd}/^{144}\text{Nd}$	0.512551	0.512630	0.512729	0.512510	0.512169	0.512547	0.512371
$\epsilon_{\text{Nd}}(0)$	-1.7	-0.2	1.8	-2.5	-9.1	-1.8	-5.2
$T_{\text{DM}}(\text{Ga})$	1.01	0.68	0.82	1.06	1.42	1.05	1.30

Table 4.3: Continued

	AND-09-49	AND-09-52	AND-09-54	AND-09-55	PB-08-08	PB-08-11	PB-08-13
(ppm)							
Rb	46.61	22.93	22.9	12.24			34.07
Sr	40.74	152.28	152.3	101.35			75.16
Ba	205.79	285.61	285.6	210.45			62.99
Y	17.20	19.32	19.3	16.85			11.27
Zr	86.11	73.52	73.5	43.30			32.21
Hf	2.88	2.82	2.8	1.68			1.49
Nb	6.81	4.13	4.1	3.26			4.27
Ta	0.47	0.24	0.2	0.19			0.33
Th	5.96	2.47	2.5	1.73			3.77
U	1.07	0.80	0.8	0.49			0.90
La	14.96	11.32	11.3	10.03			14.05
Ce	38.85	25.70	25.7	20.73			29.79
Pr	4.47	3.52	3.5	2.98			3.77
Nd	18.52	15.46	15.5	12.86			15.15
Sm	4.23	3.94	3.9	3.20			3.30
Eu	1.07	1.44	1.4	1.11			0.98
Gd	4.18	4.26	4.3	3.42			3.35
Tb	0.59	0.67	0.7	0.52			0.46
Dy	3.88	4.63	4.6	3.48			2.97
Ho	0.74	0.91	0.9	0.67			0.54
Er	2.29	2.86	2.9	2.05			1.62
Tm	0.31	0.39	0.4	0.28			0.21
Yb	2.20	2.84	2.8	1.92			1.41
Lu	0.32	0.44	0.4	0.28			0.20
Sc	17.91	18.26	18.3	17.29			5.79
V	89.67	87.34	87.3	79.07			41.82
Cr	54.88	9.54	9.5	69.00			115.20
Co	20.93	11.38	11.4	12.05			12.18
Ni	100.18	4.92	4.9	40.93			118.91
Pb	8.03	10.23	10.2	6.74			9.08
Cs	3.68	3.00	3.0	0.71			2.10
Th/Sc	0.33	0.14	0.14	0.10			0.65
Zr/Sc	4.81	4.03	4.03	2.50			5.56
La/Th	2.51	4.58	4.58	5.79			3.72
Th/Yb	2.71	0.87	0.87	0.90			2.67
$^{87}\text{Sr}/^{86}\text{Sr}$	0.71255	0.70856	0.70497	0.70554	0.71092	0.71130	0.70657
$^{143}\text{Nd}/^{144}\text{Nd}$	0.512564	0.512667	0.512833	0.512796	0.512237	0.512278	0.512604
$\epsilon_{\text{Nd}}(0)$	-1.4	0.6	3.8	3.1	-7.8	-7.0	-0.7
$T_{\text{DM}}(\text{Ga})$	1.00		0.64	0.68			0.86

Table 4.4: Trace element concentration and isotopic ratio data for siliciclastic sedimentary rocks of the Andaman Flysch Group

	AND-09-04	AND-09-12	AND-09-14	AND-09-36	AND-09-43	AND-09-61	PB-08-09
(ppm)							
Rb	89.68	75.09	81.26	90.63		90.51	
Sr	78.16	17.24	27.29	73.37		66.78	
Ba	233.74	272.72	175.35	312.93		271.06	
Y	12.56	8.61	8.79	10.55		17.75	
Zr	22.11	27.46	58.69	21.47		31.37	
Hf	1.26	1.32	2.00	1.08		1.36	
Nb	8.96	7.56	6.50	6.67		9.20	
Ta	0.61	0.50	0.43	0.55		0.67	
Th	10.62	12.35	7.09	7.58		9.90	
U	1.65	1.49	1.49	1.11		1.41	
La	29.91	26.26	20.64	22.81		38.33	
Ce	63.59	55.74	43.29	47.57		85.41	
Pr	7.53	6.58	5.16	5.79		10.37	
Nd	29.06	24.83	18.60	22.48		40.11	
Sm	5.97	4.78	3.06	4.57		8.82	
Eu	1.30	0.97	0.69	1.10		1.97	
Gd	5.45	4.11	2.75	4.11		7.73	
Tb	0.67	0.47	0.34	0.50		1.00	
Dy	3.73	2.55	2.18	2.80		5.55	
Ho	0.63	0.44	0.44	0.49		0.90	
Er	1.76	1.26	1.42	1.36		2.51	
Tm	0.22	0.16	0.20	0.17		0.31	
Yb	1.48	1.07	1.49	1.17		2.07	
Lu	0.19	0.14	0.22	0.15		0.28	
Sc	6.26	1.57	7.05	6.24		6.85	
V	49.19	15.10	90.08	48.40		59.00	
Cr	35.24	0.00	28.04	40.14		41.44	
Co	10.09	2.67	1.12	7.45		20.47	
Ni	51.17	11.58	33.49	51.99		71.95	
Pb	20.09	13.24	6.17	12.71		17.84	
Cs	5.18	3.41	5.04	4.80		4.49	
Th/Sc	1.70	7.89	1.01	1.21		1.45	
Zr/Sc	3.53	17.54	8.32	3.44		4.58	
La/Th	2.82	2.13	2.91	3.01		3.87	
Th/Yb	7.20	11.52	4.76	6.48		4.78	
⁸⁷ Sr/ ⁸⁶ Sr	0.71548	0.73049	0.71554	0.71837	0.71605	0.72323	0.72105
¹⁴³ Nd/ ¹⁴⁴ Nd	0.512142	0.511987	0.512473	0.512157	0.512059	0.512089	0.512007
ε _{Nd} (0)	-9.7	-12.7	-3.2	-9.4	-11.3	-10.7	-12.3
T _{DM} (Ga)	1.52	1.63	0.80	1.47		1.75	

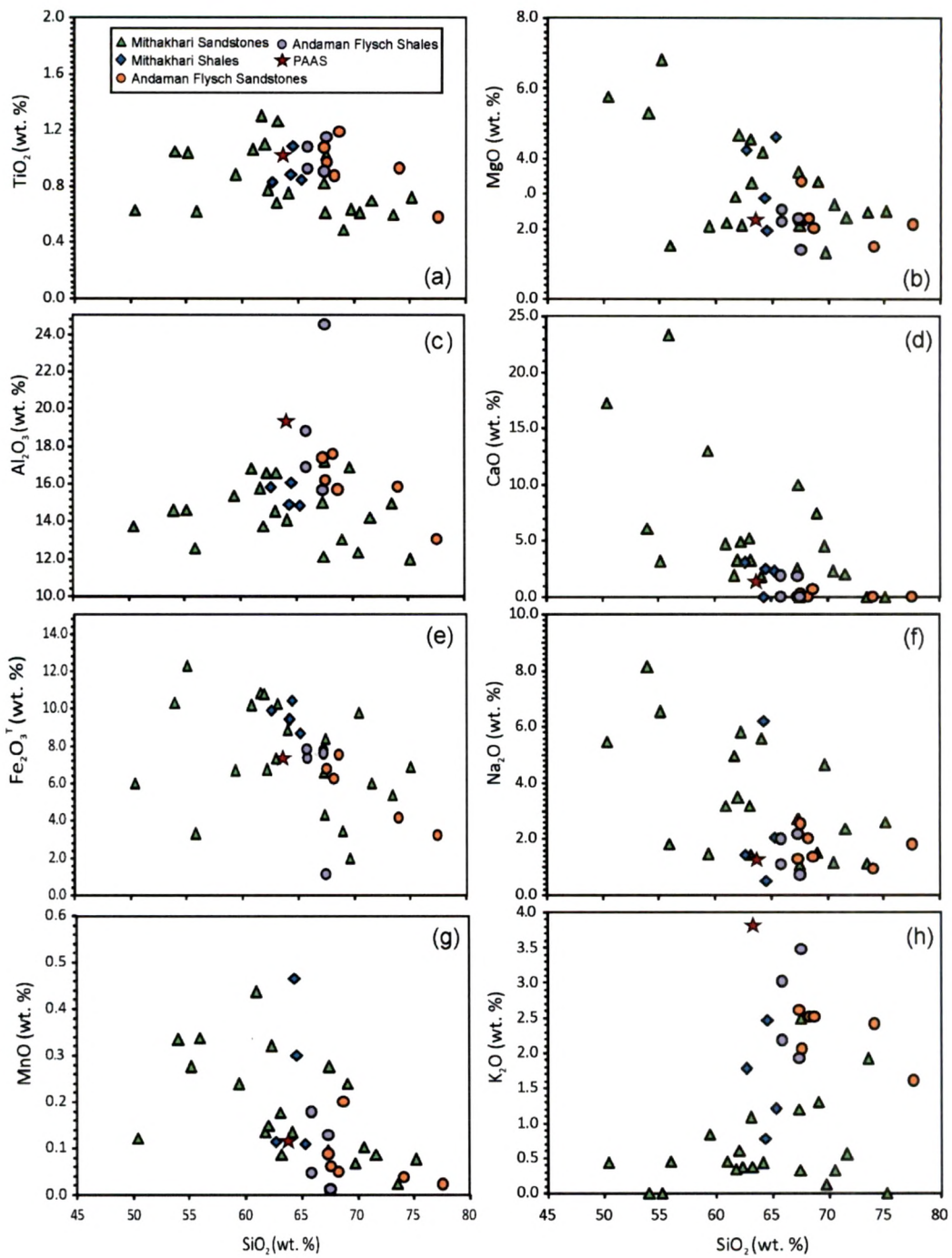


Fig. 4.4: Major element oxide versus SiO_2 for samples from the Mithakhari and the Andaman Flysch Groups. Values for PAAS are from Taylor and McLennan (1985).

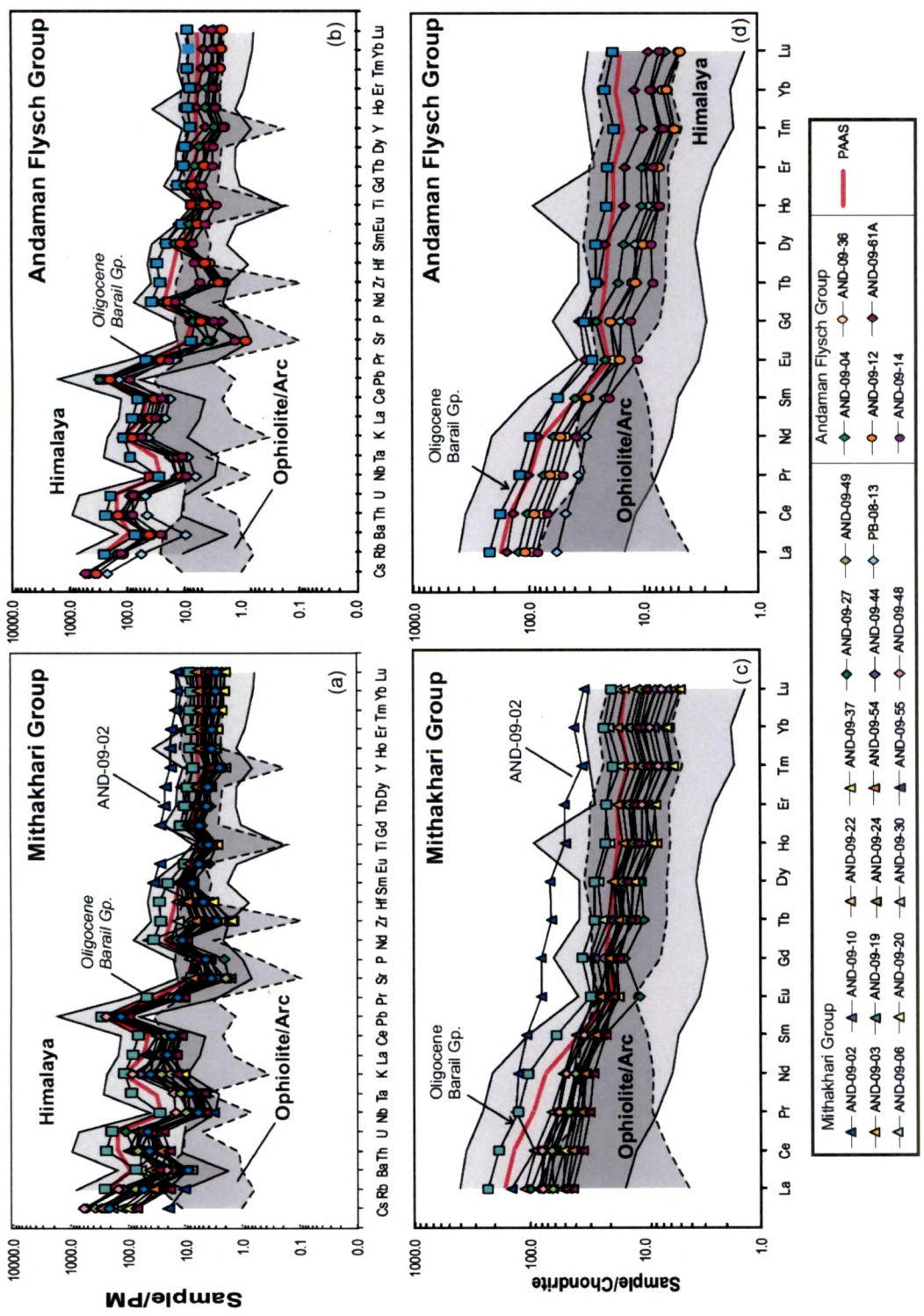


Fig. 4.5: Primitive Mantle (PM) normalized multi element spidergrams (a&b) and chondrite normalized REE patterns (c&d) for the Mithakhari Group and the Andaman Flysch Group rocks. Data Sources: PM- McDonough and Sun (1995); Chondrite- Sun and McDonough, (1989); Post Archean Average Australian shale (PAAS)-Taylor and McLennan (1985); compositions of Barail Group sediments (average)- Hossain et al., (2010); Andaman Ophiolite/Arc field- Kumar, (2011); Pal et al., (2011); Pederson et al., (2010); Himalayan field- Ahmad et al., (2000); Islam et al., (2011); Miller et al., (2001) and Sachan et al., (2010).

9. The chondrite-normalized REE patterns (Fig. 4.5c & d) for samples from the Mithakhari Group show fairly uniform, moderately enriched light REE patterns ($La_N/Sm_N = 1.4-3.6$), fairly flat HREE patterns ($Gd_N/Yb_N = 1.4-2.9$) and moderate negative Eu anomalies ($Eu/Eu^* = 0.6-1.2$) whereas those from the Andaman Flysch rocks, although, have similar features, have much higher light REE enrichment and much closer to PAAS.
10. Like other trace elements, the REE patterns for the Mithakhari rocks overlap with the field of the Andaman Ophiolites, whereas the Andaman Flysch rocks plot well within the field of Himalayan rocks (Fig. 4.5a & b).

(C) Radiogenic isotope geochemistry

The $^{87}Sr/^{86}Sr$ and $^{143}Nd/^{144}Nd$ isotopic ratios were measured on selected whole rock samples from both the Mithakhari and Andaman Flysch groups. These data are presented in Tables 4.3 and 4.4 and in histograms in Fig. 4.6. Since the Mithakhari Group rocks are better exposed and easier to access, our database is somewhat biased towards this group. Although the isotopic ratio variations in these groups overlap with each other, there exists a clear difference between the two with the Mithakhari rocks showing lower $^{87}Sr/^{86}Sr$ and higher ϵ_{Nd} (Tables 4.3 & 4.4, Fig. 4.6). The range of $^{87}Sr/^{86}Sr$ variations in the Mithakhari and Andaman Flysch groups are 0.70497 to 0.71554 and 0.71548 to 0.73049, whereas for ϵ_{Nd} these are -8.1 to +4.2 and -12.7 to -9.4, respectively. Isotopic data on these rocks from the work of Allen et al. (2007) fall well within our observed variations.

The $^{143}Nd/^{144}Nd$ isotopic ratios are used for calculation of model ages for the sedimentary rocks with respect to depleted mantle. These ages represent timings of

mantle extraction of the original igneous source rock from which the sediments were derived. However, because of multiple source contributions and sediment recycling, the

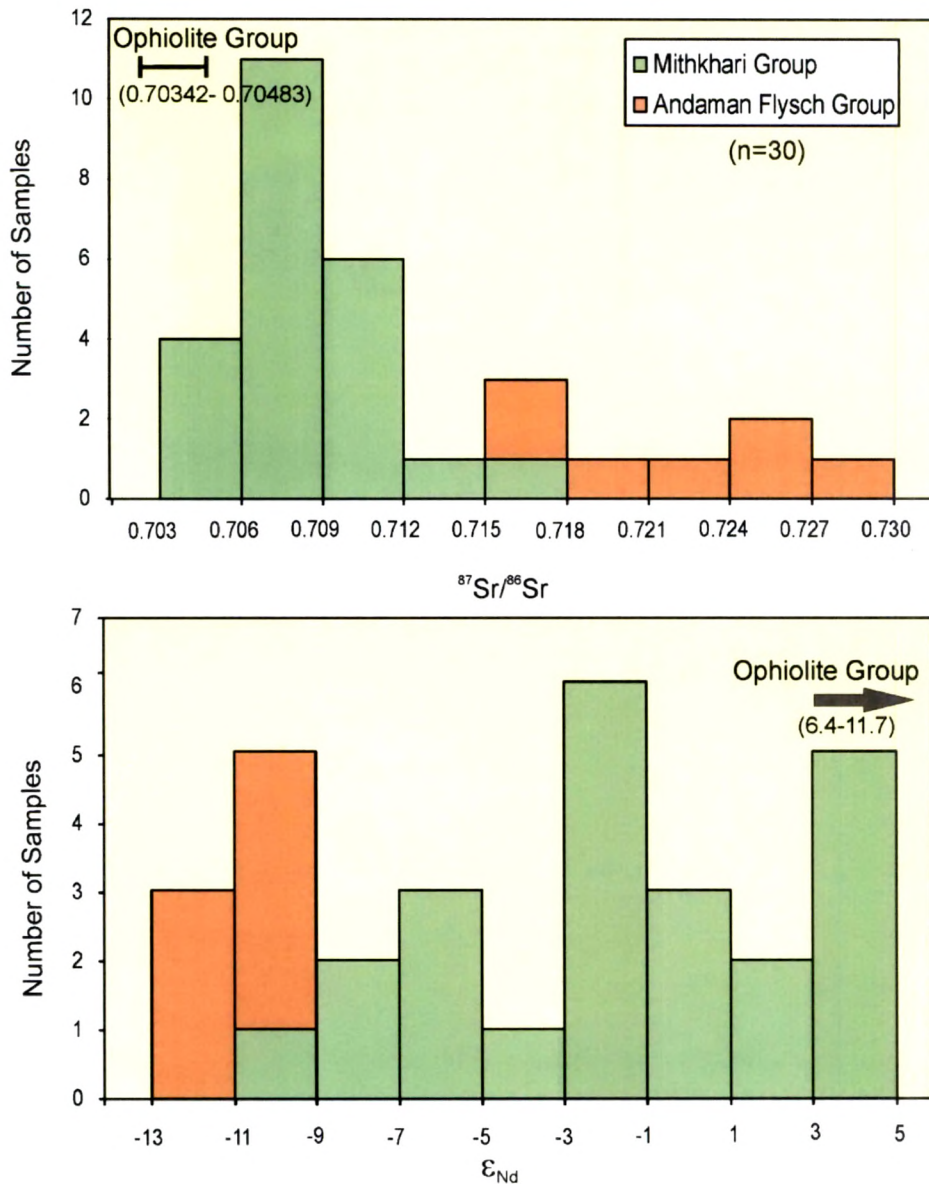


Fig. 4.6: Stacked histograms of $^{87}\text{Sr}/^{86}\text{Sr}$ and $\epsilon_{\text{Nd}}(0)$ distributions in the sedimentary rocks of the Andaman Islands. Also shown are the ranges for Andaman Ophiolites.

calculated model ages of sedimentary rocks often do not reveal the true ages of the source rocks. Usually, the ages of older terrigenous sediments decrease on getting mixed with younger sources (Faure, 2005). These ages, however, can become very helpful in understanding the provenances when used in conjunction with other tracers.

A histogram for the calculated depleted mantle ages (T_{DM}) for the Mithakhari Group and the Andaman Flysch Group rocks are shown in Fig. 4.7. The T_{DM} values for the Mithakhari Group range from 1.86 Ga to 0.57 Ga, whereas those of the Andaman Flysch Group are older. Our database, though not exhaustive, shows a prominent mode at ~ 1.1 Ga and a less pronounced mode at ~ 0.7 Ga (Fig. 4.7).

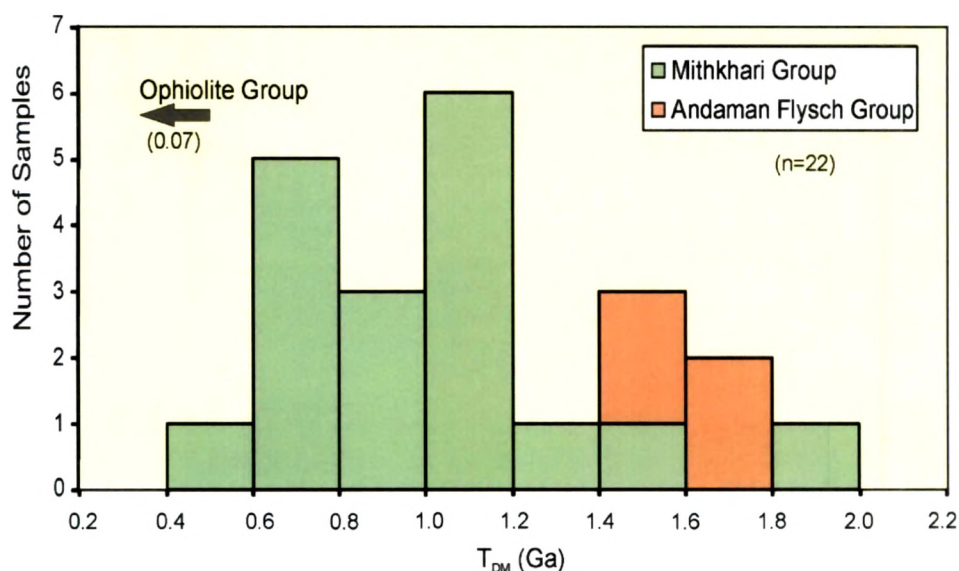


Fig. 4.7: Stacked histogram showing frequency distributions of T_{DM} ages for the sedimentary sequences of the Andaman Islands.

4.4 Discussion and Implications

4.4.1 Weathering and Sedimentation

Al_2O_3 - CaO^* + Na_2O - K_2O (A-CN-K) plot and Chemical Index of Alteration (CIA) together can be used for quantification of weathering and diagenetic history of a sedimentary rock in addition to deciphering climatic conditions during their deposition (Nesbitt and Young, 1982, 1984). As the intensity of weathering increases, the concentration of Ca, Na, and K decreases in the bulk-rock chemistry due to alteration of feldspars (and glass for volcanic rocks) into clay minerals (e.g., Duzgoren-Aydin et al., 2002; McLennan, 1993) and therefore, CIA value increases. In Fig. 4.8, all our data points plot parallel to the A-CN line suggesting variable degree of weathering of the source rocks. The CIA values for the Mithakhari Group are comparatively lower than the Andaman Flysch Group. This hints at comparatively less weathering in the sources of the Mithakhari sediments while high CIA values for the Andaman Flysch suggests high degree of weathering in their sources. Figure 4.8 also reveals out that the

sediments of the Mithakhari Group were derived from predominantly mafic igneous sources whereas plagioclase was dominant mineral and that they did not get transported long distance before deposition- which is reflected in their smectite rich clay content. In contrast, the sediments of the Andaman Flysch appear to have been derived from mixed sources with dominance of felsic igneous sources. The presence of higher amount of illite suggests that the sediments would have been transported a large distance before being deposited.

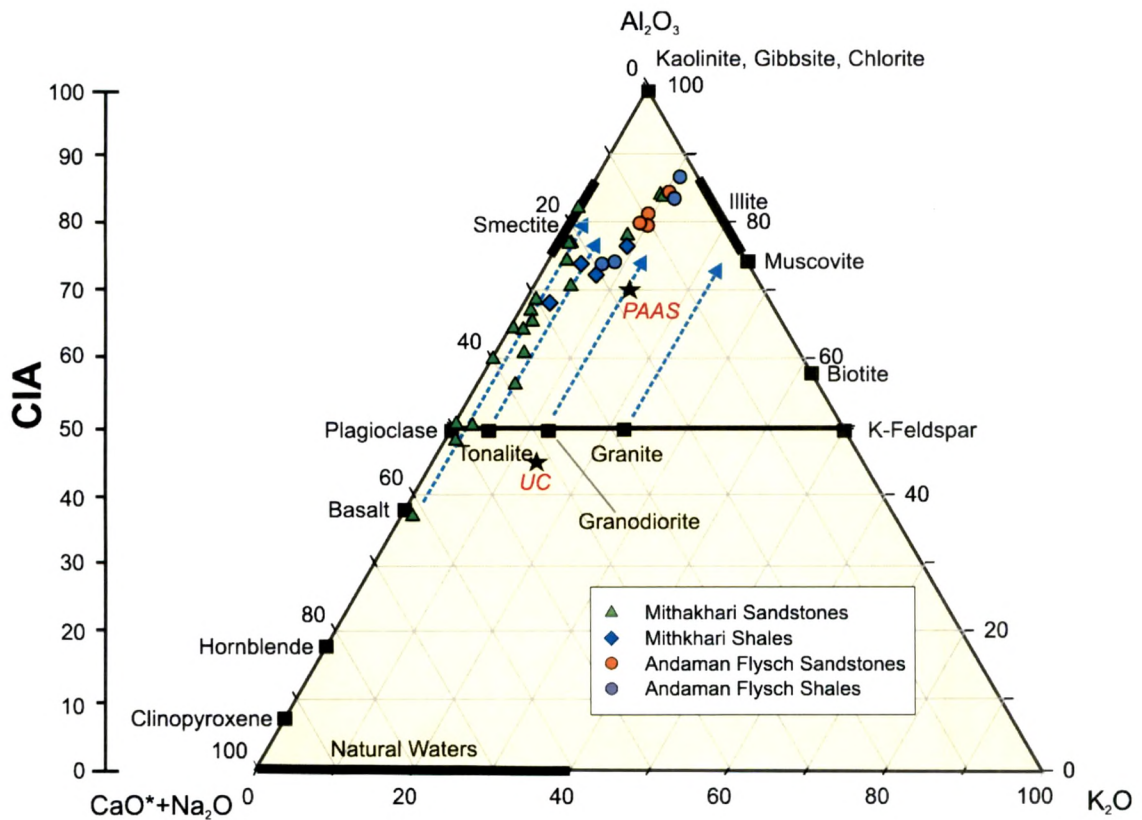


Fig. 4.8: Al_2O_3 -(CaO^*+Na_2O)- K_2O diagram with the Chemical Index of Alteration (CIA) of Nesbitt et al. (1996) on which samples from the Andaman sedimentary rocks are plotted. Also shown on the diagram are the positions of characteristic minerals, post-Archean Australian Average Shale (PAAS) (Taylor and McLennan, 1985), and average Archean upper crust (Taylor and McLennan, 1985). The solid and dashed lines with CIA values for shales have CIA values to the range of 70-75. Arrows emanating from plagioclase-K-feldspar join show the weathering trends for basalt, tonalite, granodiorite and granite (Nesbitt and Young, 1984, 1989).

Th/Sc is a good indicator of igneous differentiation process and Zr/Sc ratio gives a measure of mineral sorting and recycling (Hassan et al., 1999), therefore, a plot of Th/Sc versus Zr/Sc in sediments can provide clues about the nature of their sources and

processes of removal of material out of them (McLennan, 1993). In such a plot (Fig. 4.9) the Mithakhari Group rocks show low Th/Sc and Zr/Sc ratio suggesting that sediment have not undergone much recycling and sorting. In comparison, the Andaman Flysch Group rocks have relatively higher Th/Sc and Zr/Sc ratios with values above the average value of the upper continental crust (Fig 4.9) suggesting that they have undergone substantial recycling and sorting, and have concentrated zircons during transport.

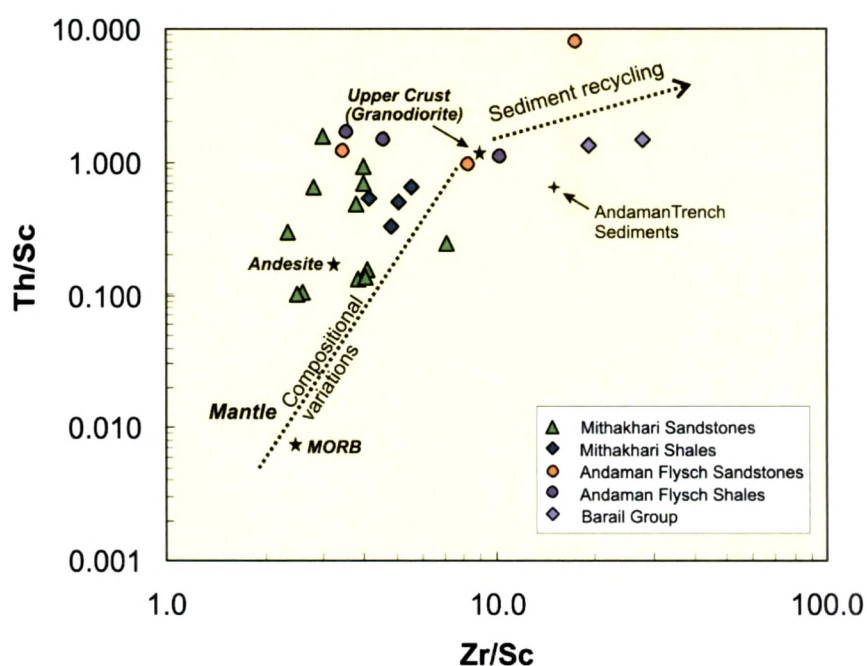


Fig. 4.9: Plot of Th/Sc versus Zr/Sc for Andaman Island samples. Also plotted are ratios for upper crust (Taylor and McLennan, 1985) and Andaman Trench sediments (Planck and Langmuir, 1998).

The chemical composition of sedimentary rocks show close link to tectonic environments and provenance as long as it is not disturbed/modified during post-depositional processes. The tectonic and sedimentary processes impart a distinctive geochemical signature to sediments and different tectonic environments have distinctive provenance characteristics (Bhatia and Crook, 1986). In two such tectonic discrimination plots of K_2O/Na_2O versus SiO_2 and La-Th-Sc ternary diagram, the data from the Andaman sedimentary formations predominantly fall in the fields of island arc and active continental margin (Fig. 4.10). While the Mithakhari Group rocks, barring a

few, show chemical signatures of island arc setting, the Andaman Flysch rocks clearly were deposited in a predominantly active continental margin setting (Fig. 4.10).

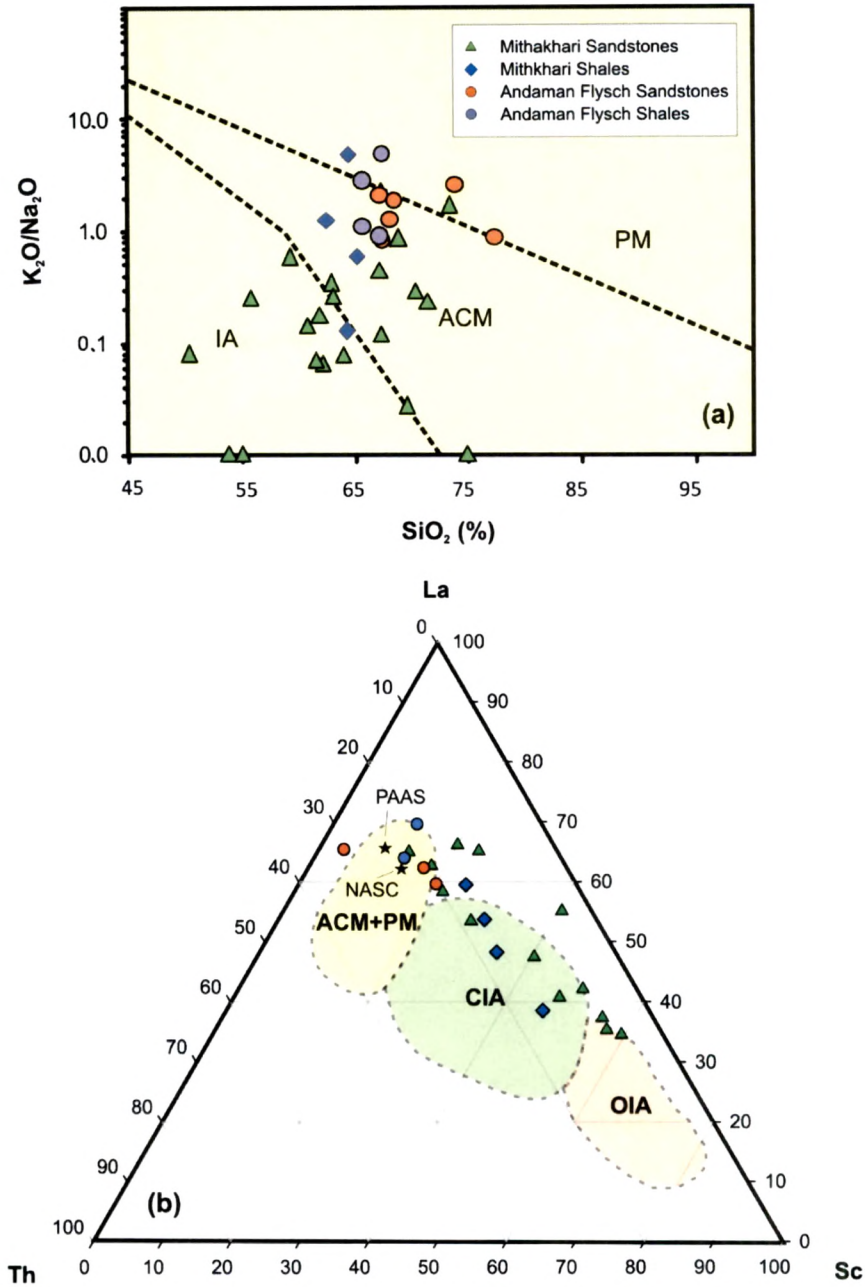


Fig. 4.10: (a) K_2O/Na_2O versus SiO_2 discrimination diagram of Roser and Korsch (1986) for sediment of the Mithakhari Group and the Andaman Flysch Group. Fields shown are for passive continental margin (PM), an active continental margin (ACM) and island arc (IA) (b) La-Th-Sc discrimination diagram of Bhatia and Crook, (1986) for the same sediments. Fields shown are for oceanic island arc (OIA), continental island arc (CIA), passive continental margin (PM) and active continental margin (ACM). Values for PAAS are from Taylor and McLennan, (1985).

4.4.2 Provenance

Chemical compositions of siliciclastic sediments have been widely used as indicators of provenances (e.g., McLennan et al., 1995, 2003). The elemental abundances (and ratios) of relatively immobile elements (REE, Th, Nb, Sc & Zr) remain unchanged during weathering and diagenesis processes. Therefore, these elements get transferred quantitatively from parent rocks to the clastic sediments produced from them (Taylor and McLennan, 1985; Condie, 1991). In the primitive mantle-normalized multi element spidergrams and chondrite-normalized REE plots (Fig. 4.5) the Mithakhari Group samples show larger contribution of sediments derived from the suprasubduction ophiolites of the Andaman Subduction Zone while the Andaman Flysch sediments with their relatively enriched LREE patterns appear to have been derived primarily from the Himalayan rocks, having crustal signatures.

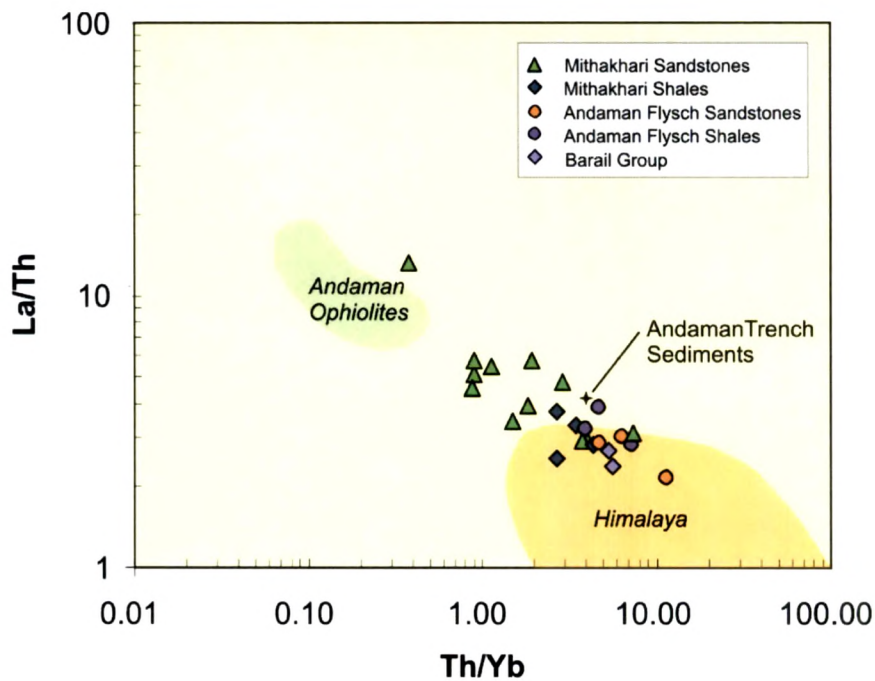
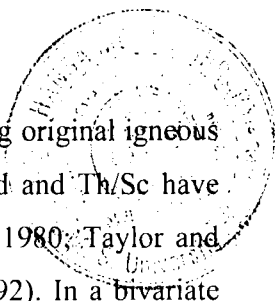


Fig. 4.11: *La/Th* and *Th/Yb* variations in sandstones and shales from the Mithakhari Group and the Andaman Flysch Group. The Andaman Ophiolite field is drawn using data from Pal et al. (2011) and Pederson et al. (2010) while Himalayan field is drawn using those from Ahmad et al. (2000); Islam et al. (2011); Miller et al. (2001) and Sachan et al. (2010); Andaman Trench sediments-Planck and Langmuir (1998).

Because of their relative incompatibility during differentiation of mafic and felsic igneous rocks, the concentration of elements La, Th and Sc vary widely in various



magmatic rocks and therefore, can become very useful in determining original igneous sources for sediments. The ratios like La/Th, La/Sc, Th/Yb, Sm/Nd and Th/Sc have been successfully used as tracers of provenance (McLennan et al., 1980; Taylor and McLennan, 1985; Wang et al., 1986; McLennan and Hemming, 1992). In a bivariate plot between La/Th versus Th/Yb (Fig. 4.11) sedimentary rocks from the Andamans plot in-between the fields for the Ophiolite Group of the Andamans and rocks of the Himalayan mountain belt, which suggest that these sediments are a mixture of materials derived from these two sources. As observed in the A-CN-K plot (Fig. 4.8), the majority of the Mithakhari Group formations follow a trend that suggest their derivation from mafic igneous sources (basaltic), while rocks from the Andaman Flysch Group and a few sandstone and shale formations of the Mithakhari Group follow a granodiorite trend, suggesting dominance of continental/felsic material over in their sources.

$^{143}\text{Nd}/^{144}\text{Nd}$ is a robust tracer for determining sediment source in comparison to $^{87}\text{Sr}/^{86}\text{Sr}$ because it is not susceptible to alteration during weathering and diagenesis (Patchett, 2003). In addition, the parent-daughter ratio of Sm-Nd systematics is highly resistant during diagenesis unlike mobile Rb and Sr. However, considering that the rocks of the Andaman Islands are young (< 100 Ma) and that the samples studied for isotopic composition are devoid of carbonate cements, we believe that their $^{87}\text{Sr}/^{86}\text{Sr}$ too can help us trace the sediment sources.

Comparing the observed ϵ_{Nd} variations in Andaman sedimentary rocks with that of the possible sources (Fig. 4.12a) we make the following observations. The Mithakhari Group rocks show large variation in ϵ_{Nd} which supports our earlier inference that their sediments have variable mixing from arc and continental sources. We also observe that there is a progressive lowering of ϵ_{Nd} with younging, which ends up with more negative values for the Andaman Flysch rocks; suggesting predominant contributions from continental sources in younger rocks. To quantify the amounts of contributions from these above two sources (i.e. magmatic Arc/ophilitic and continental crust) we utilized both Sr and Nd isotopic ratios.

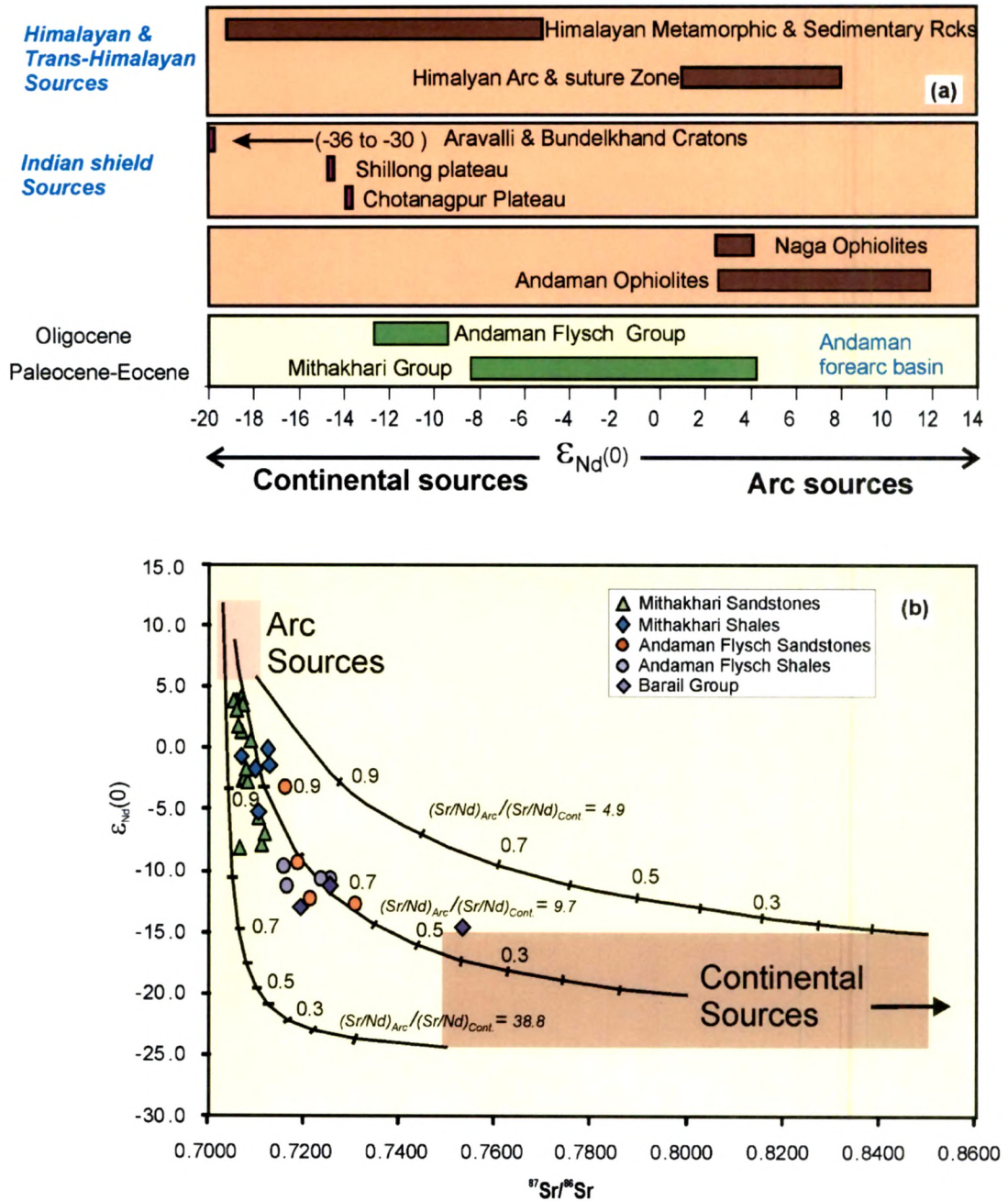


Fig. 4.12: (a) Plot of $\epsilon_{Nd}(0)$ ranges observed in the Mithakhari Group and the Andaman Flysch Group compared with data from possible source regions (as given in Allen et al., 2007; Allen et al., 2008; Najman et al., 2008). (b) Plot of $\epsilon_{Nd}(0)$ versus $^{87}Sr/^{86}Sr$ for our samples and sediments from the Barail Group of Bengal Basin compared with two component mixing model curves that assume three different end-member pairs for Arc and Continental sources. The tick marks on the mixing curves represent fraction of Arc source material in the mixture. Data sources: Andaman Island ophiolites: Kumar (2011), Barail Group sediment: Najman et al., (2008). All data were normalized to NBS987 (0.710250) and La Jolla (0.511858) for $^{87}Sr/^{86}Sr$ and $^{143}Nd/^{144}Nd$ isotopic ratios, respectively.

In a ϵ_{Nd} versus $^{87}Sr/^{86}Sr$ diagram (Fig. 4.12b) we plot our data and compare them with the potential sources: the rocks of the Andaman Ophiolite Group and the magmatic arc, and rocks of the upper continental sources (e.g., in our case these could have been the rocks of the Indian Shield and the Himalayas). As can be seen in the Fig. 4.12b the rocks of the Mithakhari Group, with their higher ϵ_{Nd} and lower $^{87}Sr/^{86}Sr$, plot closer to the magmatic arc sources, whereas the rocks of the Andaman Flysch Group, with their lower ϵ_{Nd} and higher $^{87}Sr/^{86}Sr$ plot away from it but are closer to values for upper continental crustal material. All the sedimentary rocks appear to show a mixing trend (hyperbola) between the above two end member sources. Considering that the most probable upper continental crustal end-member in this case is the sources in the Himalayas and the magmatic arc member is local (Andaman ophiolites), we draw simple binary mixing curves, using three different end-member pairs, to explain the observed data. The results of mixing calculations reveal that the local arc sources possibly contributed >80% of sediments to the Mithakhari Group, whereas the same sources contributed about 60-80 % to the Andaman Flysch. The maximum amount of continental contribution to the rocks of the Andaman forearc basin could not have exceeded 30% of the total. Interestingly, we also find that the sediments of the Barail Group in the Bengal Basin too had received significant amount of sediments ($\leq 30\%$) from the arc sources, probably those located in Myanmar.

Presence of mafic-ultramafic clasts in the basal conglomerate and interbedded tuff deposits, and results of our geochemical study all indicate that the local ophiolites along with volcanic arc acted as the major sources for sediments to the Mithakhari Group. The suprasubduction ophiolites present in the Andamans were probably subaerially exposed during the early to middle Eocene and had undergone substantial erosion. This process produced clasts with weakly weathered coarse sediments which were locally deposited within the trench-forearc basin. The tectonic plate configuration at this time possibly allowed transport of additional sediments from the Himalayan/Indian Shield sources into this basin.

Results from petrography (this study; Pal et al., 2003; Allen et al., 2007), geochemical and isotopic studies indicate that distant felsic continental rocks acted as the main

sources of sediments to the Andaman Flysch Group. Presence of Archean, Proterozoic, and Paleozoic age zircons corroborates this (Allen et al., 2007). These sediments apparently have a complex weathering and transportation history. All evidences support our inferences that these sources were located either in the rising Himalayan mountain belt or in the eastern Myanmar region. Although, it is difficult to discriminate between the two, the absence of major drainage system in eastern Myanmar, capable of transporting large amounts of sediments led us to believe that the Himalayan-Transhimalayan sources were the primary provenance for the Oligocene forearc deposits.

4.4.3 Evolution of the Andaman region

Based on the inferences made above on the provenance of the Andaman sediments and our understanding of the paleogeography and paleodrainage systems that might have existed in the continents surrounding the forearc during the Paleogene, we propose certain tectonic configurations of SE Asia at ~50 Ma and ~30 Ma in Fig. 4.13. We believe that the terminal phase of continental collision between the Indian and Eurasian plates happened at ~50 Ma (Rowley, 1996; Hodges, 2000). A remnant of the Neo-Tethys Sea probably existed at this time north of the Himalayan suture zone (Fig. 4.13). On further movement of the Indian plate to the north during the Early Eocene, this narrow sea might have started closing from the west. The Trans-Himalayan-Sunda magmatic arc existed parallel to the collision-subduction boundary. The first ~12 Myr of post-collisional sedimentary record (i.e. until about 38 Ma) from the foreland basin, Bengal basin and the Andaman forearc basin show negligible input of sediments from continental sources but have substantial contributions from magmatic arc/suture zone sources (Najman and Garzanti, 2000; Najman et al, 2008). Figure 4.13a illustrates the paleogeographic configuration at ~50 Ma and shows the direction of sediment transportation from arc/suture zone sources into the Bengal basin and Andaman forearc through paleodrainage systems. The dominance of arc/suture zone sources suggests that until that time, the Himalayas had not attained the critical height for large scale weathering. In addition, the SW monsoon system did not exist, which otherwise would have aided the erosion and transportation of sediments from the Indian Shield and nascent Himalaya.

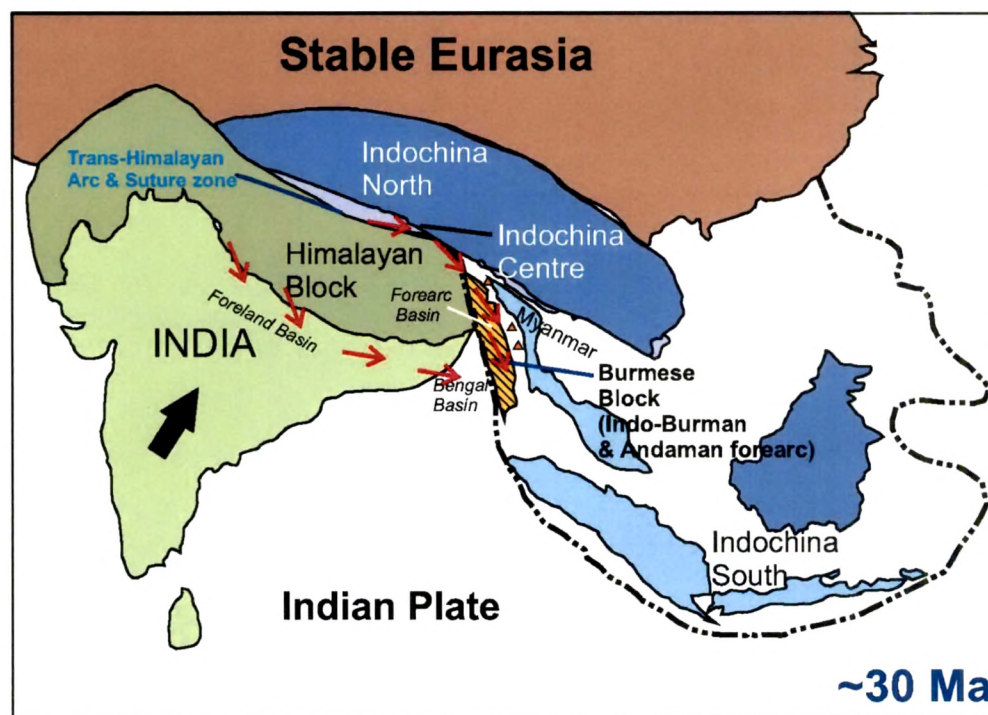
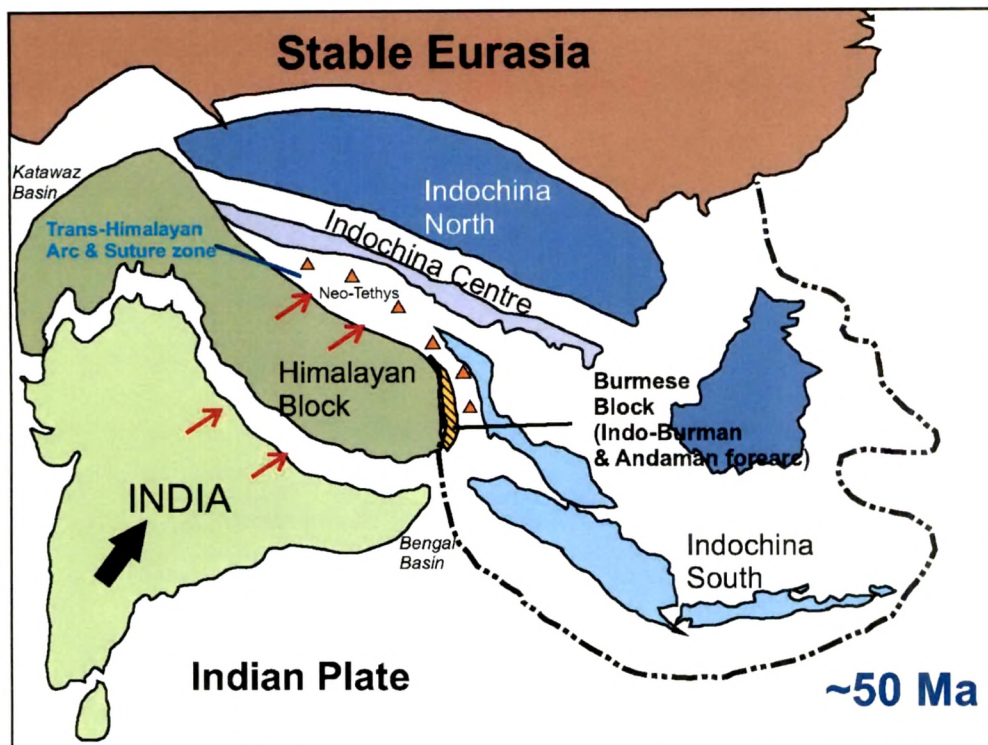


Fig. 4.13: Schematic maps showing the Paleogene configuration of the Indian Plate and other tectonic blocks of SE Asia at 50 Ma and 30 Ma (modified after Replumaz and Tapponnier, 2003). The Greater India moved northward throughout the Paleogene with crustal shortening at its northern margin. The sketch also illustrates the location of volcanic arc (triangles) and continental sources and paleodrainage directions (arrows) to the forearc and foreland basins.

We believe that at ~40 Ma, major thrusting events occurred along the northern continental margin of the Indian plate. This probably provided sufficient topographic barrier to the moisture from the south and resulted in the development of the first monsoon system. The monsoon enhanced the weathering and erosion of the exhumed continental crust and resulted in exponential increase in the sediment input to the adjacent basins at the start of the Oligocene (Metivier et al., 2002). From the Oligocene onwards the major input of Himalayan detritus was deposited in the Bengal Basin and also in the Andaman forearc basin. The volume of sediments deposited suggests that the exhumation and erosion of the Himalaya that occurred during the Oligocene was rather more intense and covered a larger spatial extent than previously thought. This suggests that the some major river systems had already developed and was supplying sediments to these basins from the north or northeast and west. We believe that these sediments were supplied by the paleodrainage system of the Ganga draining into the foreland basin through the southern slopes of the rising Himalaya and that of Yarlung-Tsangpo River (Tibet) developed in the Himalayan arc and suture zone with the closing of the Neo-Tethys (Fig. 4.13b). The now exposed Indo-Burman ranges and Andamans were part of the same forearc basin. With continued subduction in its western part, these trench-forearc deposits of the Indo-Burman block started uplifting during the Oligocene to form the Indo-Burman Ranges (Mitchell, 1993). This upliftment of Indo-Burman Ranges must have acted as a barrier to the drainage system and divided it into two parts- the Brahmaputra River system carrying sediments to the Indian plate and Irrawaddy River system on the Burmese plate. The Ganga and Brahmaputra river systems supplied sediments to the Bengal basin and Bay of Bengal while the Irrawaddy river system supplied sediments to basins to the further east.

Tectonic activities continued the upliftment of trench-forearc sediments which progressed from the north to the south. This first exposed the Indo-Burman Ranges and later the (islands of) Andamans. A major episode of uplift at ~20 Ma, believed to be a result of major tectonic events (Allen et al., 2007; Mountain and Prell, 1990; Acharyya et al., 1989), terminated the deposition of the Andaman Flysch Group and probably shifted the centre of deposition further west to the Bay of Bengal. To the east of the raised ophiolite and trench-forearc sequences deposition of the Archipelago Group sediments started in deep marine conditions (Pal et al., 2005; Singh et al., 2000). Allen

et al. (2007) suggested that the present topography of the Andaman Islands is resulted from a major regional upliftment event that occurred during ~ 10 to 5 Ma. The subduction continued in the west of the Andaman Islands and the Andaman Sea opened in the east during the Late Miocene to Pliocene (Curry, 2005).

4.5 Provenance of sediments of the Andaman Sea

4.5.1 Background and Earlier work

The Andaman Sea receives more than 360 million tonnes of sediment from the surrounding landmasses annually (Meade, 1996; Milliman and Meade, 1983). Earlier studies have shown that a large portion of this sediment supply is delivered by the tropical/subtropical river systems of Myanmar; notably the Irrawaddy, Sittang and Salween with the first being the dominant of all (Rodolfo, 1969) (Fig. 4.14). The Irrawaddy River is the fifth largest in the world in terms of sediment discharge (Rao et al., 2005). The reason for such a high influx of sediment is higher monsoonal rainfall and resultant erosion in the drainage basins. Along with the Indian subcontinent, Myanmar is affected by South Asian Monsoon, which comprises the South West (summer) and the North East (winter) monsoons. Both these monsoons play an important role in the erosion in the catchments of these rivers. The sediment load in the Irrawaddy River system is derived from: the Himalayas in far north, Indo-Burman mountain ranges in the west and Shan Plateau in the east (Fig. 4.14) (Robinson et al., 2007). Although the exact amounts of sediment loads contributed by each of these sources are unknown, the study by Allen et al. (2007) suggests these to be a complex mixture of sediments derived from multiple sources. In Table 4.1, we describe important physical and chemical characteristics of these sediment sources. The Indo-Burman sources are similar to those occur on the Andaman Islands and mainly are ophiolites, volcanoclastics and siliciclastic sedimentary rocks of Cretaceous to Oligocene age (Allen et al., 2008; Colin, 2006).

The Andaman Sea is characterized by a seasonally reversing surface circulation pattern linked to the monsoons. The sediment load brought in by the rivers is supplied to it from the north, of which most get deposited on the broad continental shelf in the gulf of Martaban while rest are carried to the east and south along the continental shelf of

Myanmar and Thailand by the coastal currents driven by SW monsoonal winds (Rodolfo, 1969).



Fig. 4.14: Map showing (sediment) source regions and major rivers of Myanmar (source: [http://en.wikipedia.org/wiki/File: Myanmar_relief_location_map.jpg](http://en.wikipedia.org/wiki/File:Myanmar_relief_location_map.jpg)).

Only a small part of the sediment supplied finally reaches to the deeper parts of the Andaman Sea. These coastal currents reverse their direction during the NE monsoon

and carry sediments westward towards the Bay of Bengal (Ramaswamy et al., 2004; Rao et al., 2005) (Fig. 4.15). Apart from the major sediment contribution from north, there is also some minor contribution from Malay Peninsula, however, its deposition is limited only to the inner shelf (Rodolfo, 1969). The sediments deposited in the south and south-east Andaman Sea, which are probably derived from sources in Malay Peninsula and Sumatra, are carried by the Malacca currents into the Bay of Bengal (Rodolfo, 1969) (Fig. 4.15).

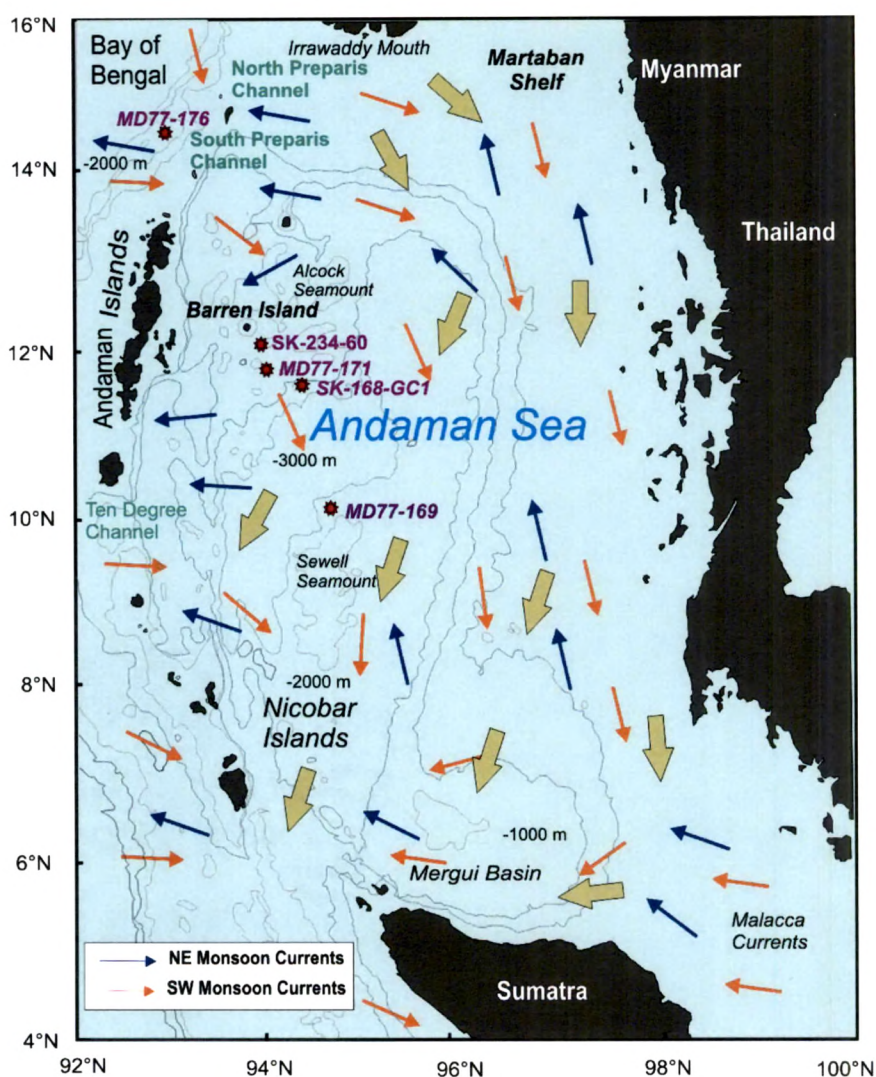


Fig. 4.15: Map of the Andaman Sea (source: http://www.internalwaveatlas.com/Atlas_PDF/IWAtlas_Pg207_AndamanSea.PDF) showing bathymetry and location of sediment cores SK-234-60, SK 168/GC-1 MD77-169, MD77-171 and MD77-176. Blue arrows are directions of North-East (winter) monsoon currents while orange arrows are South-West (summer) monsoon currents (Rodolfo, 1969), Thick yellow arrows show direction of sediments carried by currents.

The intensity of the monsoons has been known to have varied in millennial scale during the late Pleistocene and Holocene (Duplessy, 1982; Herzschuh, 2006; Prell and Kutzbach, 1987; Sarkar et al., 1990; Tiwari et al., 2005). Such fluctuations are mainly controlled by the low latitude solar insolation, which varied with precession and eccentricity of the Earth's orbit (Clemens and Prell, 1990; Clemens et al., 1991; Colin et al., 1998; Duplessy, 1982). Several studies have shown that past variations in the South-East Asian monsoonal intensity have influenced erosion and caused major changes in the sediment supply (e.g., Tripathy et al., 2011). These also affected seawater circulation and sediment dispersal pattern in the Indian Ocean (Hashimi et al., 1995; Goodbred and Kuehl, 2000; Colin et al., 1999). Therefore, it is expected that temporal changes in monsoon intensity in the past could have brought major changes to the weathering-erosion pattern in the source regions (of Myanmar) for the sediments to the Andaman Sea. Unfortunately, due to lack of detailed studies in the S-E Asia, we know very little about how sediment contribution to the Andaman Sea varied with time as a result of climatic fluctuations. In this work, we have made an effort to understand the relationship between variations in provenance of terrigenous sediments to the Andaman Sea and monsoon aided erosion in the source regions in the South-East Asia and Indian shield, during the late Pleistocene and Holocene, with the help of geochemical and isotopic tracers in a sediment core collected from the Andaman Sea.

4.5.2 Results

The sediment core (SK-234-60) which was raised from the western Andaman Sea from the location N12°16'40", E93 ° 51'30" to study the history of volcanism of Barren Island was utilized for this work as well. The sampling and chronological details of the core have already been discussed in Chapter-2 and Chapter-3, respectively. The geochemical and Sr-Nd isotopic data for the carbonate free siliciclastic sediments are presented in Table 4.5.

(A) C-14 ages and sedimentation rates

The AMS C-14 ages obtained for different sediment layers in the core (Tables 3.1) were used for calculation of sedimentation rates (Fig. 3.3). Our calculations yielded the following rates of sedimentation: 6.1 ± 0.4 cm/kyr during 2.2-3.8 ka, 7.3 ± 0.7 cm/kyr during 3.8-5.2 ka, 8.3 ± 0.8 cm/kyr during 5.2-6.4 ka, 7.5 ± 0.4 cm/kyr during 6.4-8.0 ka,

3.7±0.1 cm/kyr during 8.0-12.3 ka, 3.0±0.1 cm/kyr during 12.3-17.3 ka, 2.4±0.1 cm/kyr during 17.3-23.5 ka, 3.5±0.1 cm/kyr during 23.5-34.4 ka, and 5.5±0.7 cm/kyr prior to 39.5 ka (Fig. 3.4). The errors, at 1 σ level, on the above rates were determined by propagating the errors on the ages. The average sedimentation rate in the core estimated to be 5.3 cm/kyr, is much lower than earlier estimates of average sedimentation rate in the Andaman Sea: 15 cm/kyr (Frerichs, 1968), 10cm/kyr (Core MD77-169 from the Sewell seamount region; Colin et al., 2006) and 7.8 cm/kyr (from Alcock Seamount region; Sijinkumar et al., 2010) (Fig. 4.15).

The lower sedimentation rate at our core site could be due to the unusual local bathymetry and easterly flowing surface currents that disperse sediments more towards eastern continental margin than to straight south (Fig. 4.15). Linear extrapolation of calculated rate of sedimentation from bottommost dated band gives the age of bottom of the core to be ~74 ka (Fig 3.4). The depth-age model for the core is used to infer about the temporal variation of the sources supplying sediments to the core location.

(B) Geochemical Data

Based on major and trace element contents of the siliciclastic sediments from various layers of the core we make the following observations.

1. The SiO₂ contents of the analysed sediments varied between 48 and 61% and Al₂O₃ concentrations were always >15%.
2. The K₂O/Na₂O contents varied between 0.25 and 2.44.
3. The abundances of CaO in the samples varied between 1 and 6%.
4. The primitive mantle normalized trace element concentration data for the sediments (Fig. 4.16) show strongly depleted Nb and Ta patterns. Depletions in Sr and Zr are also observed in many samples. Enrichments in Th, U and Pb are prominent.
5. The concentrations of most of the elements, except for Nb, Ta and Pb, in the sediments of the core overlap with that observed in sediments in the Irrawaddy and Ganga-Brahmaputra river systems. Nb, Ta and Pb contents in sediments from top layers of the core mimic the pattern observed in island arc lavas from Barren Island (Fig. 4.16a).

Table 4.5: Geochemical and isotopic data for sediments from core SK-234-60

Sample code	SL-1 (0-5 cm)	SL-2 (15-20)	SL-3 (20-25)	SL-4 (30-35)	SL-32 (40-45)	SL-5 (55-60)
Mean Depth (cm)	2.5	17.5	22.5	32.5	42.5	57.5
(wt. %)						
SiO ₂				60.79		61.66
TiO ₂				0.81		0.86
Al ₂ O ₃				17.66		17.31
Fe ₂ O ₃ ^T				7.16		6.67
MnO				0.07		0.07
MgO				3.87		3.93
CaO				5.20		4.91
Na ₂ O				2.99		3.46
K ₂ O				1.37		1.07
P ₂ O ₅				0.07		0.07
CIA				64.87		64.69
K ₂ O/Na ₂ O				0.46		0.31
(ppm)						
Rb	39.10	43.35	49.56	108.42		78.09
Sr	150.63	162.16	133.28	63.85		81.21
Ba	154.64	226.51	259.98	351.85		281.98
Y	15.80	16.01	14.07	8.49		12.94
Zr	53.90	51.63	50.53	43.40		65.66
Hf	1.88	1.74	1.74	1.94		2.25
Nb	1.44	1.71	2.11	4.98		4.37
Ta	0.14	0.16	0.20	0.40		0.43
Th	3.32	3.82	4.35	9.44		6.45
U	0.53	0.57	0.62	1.00		1.04
La	6.53	7.50	8.19	13.56		11.30
Ce	14.72	16.51	17.51	25.83		22.41
Pr	1.91	2.10	2.19	3.09		2.76
Nd	8.33	8.91	8.97	11.57		10.67
Sm	2.21	2.25	2.18	2.35		2.35
Eu	0.86	0.83	0.78	0.70		0.70
Gd	2.63	2.60	2.44	2.33		2.47
Tb	0.43	0.42	0.38	0.33		0.37
Dy	3.19	3.05	2.78	2.36		2.65
Ho	0.66	0.62	0.57	0.49		0.55
Er	2.17	2.02	1.88	1.61		1.79
Tm	0.30	0.29	0.26	0.23		0.25
Yb	2.21	2.05	1.90	1.70		1.88
Lu	0.34	0.32	0.29	0.26		0.28
Sc	24.44	24.62	21.07	16.22		22.10
V	216.75	210.45	179.86	118.18		171.81
Cr	70.91	79.77	72.69	66.38		72.07
Co	14.51	16.31	12.27	6.44		6.88
Ni	38.67	49.68	47.44	47.73		55.55
Pb	5.94	10.58	6.26	7.15		7.92
Cs	3.34	3.77	4.39	10.19		7.36
La/Th	1.97	1.96	1.88	1.44		1.75
Th/Yb	1.50	1.86	2.29	5.55		3.43
Th/Sc	0.14	0.16	0.21	0.58		0.29
Th/U	6.28	6.73	6.97	9.45		6.18
Sm/Nd	0.26	0.25	0.24	0.20		0.22
Eu/Eu*	1.05	1.02	1.00	0.89		0.86
⁸⁷ Sr/ ⁸⁶ Sr	0.70531	0.70600	0.70629	0.70944	0.70967	0.70791
¹⁴³ Nd/ ¹⁴⁴ Nd	0.512691	0.512629	0.512566	0.512354	0.512234	0.512435
ε _{Nd} (0)	1.0	-0.2	-1.4	-5.5	-7.9	-4.0
T _{DM} (Ga)	1.04	1.07	1.11	1.17		1.16

Major element oxide data are normalized to 100% on a volatile free basis. CIA = $[\text{Al}_2\text{O}_3 / (\text{Al}_2\text{O}_3 + \text{K}_2\text{O} + \text{Na}_2\text{O} + \text{CaO}^*)] 100$ where CaO* represents CaO in silicate fractions. SL: Sediment Layer.

Table 4.5: Continued

Sample code	SL-6 (65-70)	SL-7 (75-80)	SL-8 (85-90)	SL-9 (95-100)	SL-10 (105-110)
Mean Depth (cm)	67.5	77.5	87.5	97.5	107.5
(wt. %)					
SiO ₂	60.28	61.05	63.00		62.58
TiO ₂	0.93	0.82	0.92		0.90
Al ₂ O ₃	17.02	17.67	19.93		18.56
Fe ₂ O ₃ ^T	6.95	5.95	6.09		6.43
MnO	0.07	0.06	0.05		0.08
MgO	2.85	3.77	3.21		3.10
CaO	5.09	5.67	2.94		4.57
Na ₂ O	3.98	3.71	1.85		2.18
K ₂ O	1.13	1.21	1.93		1.55
P ₂ O ₅	1.70	0.08	0.06		0.05
CIA	62.54	62.51	74.77		69.09
K ₂ O/Na ₂ O	0.28	0.33	1.05		0.71
(ppm)					
Rb	30.89	89.54	124.74	54.97	92.96
Sr	303.29	69.46	65.70	180.37	95.40
Ba	133.35	281.82	347.39	179.26	222.42
Y	11.00	9.22	9.97	18.77	12.26
Zr	7.39	50.93	64.70	48.59	67.58
Hf	0.60	1.87	2.11	1.82	2.15
Nb	0.89	4.53	6.90	2.49	5.08
Ta	0.07	0.35	1.67	0.21	0.37
Th	5.55	7.04	9.85	4.55	6.68
U	6.78	1.04	1.49	2.74	1.05
La	11.05	12.10	16.30	11.34	12.28
Ce	24.98	23.30	31.06	25.59	24.35
Pr	2.83	2.81	3.64	3.19	2.93
Nd	11.17	10.53	13.35	13.44	11.08
Sm	2.56	2.13	2.51	3.38	2.33
Eu	0.61	0.65	0.66	1.00	0.70
Gd	2.63	2.08	2.30	3.77	2.37
Tb	0.38	0.30	0.31	0.58	0.35
Dy	2.49	2.10	2.11	3.96	2.47
Ho	0.48	0.43	0.44	0.79	0.51
Er	1.48	1.41	1.45	2.47	1.68
Tm	0.20	0.20	0.21	0.33	0.25
Yb	1.42	1.47	1.54	2.39	1.75
Lu	0.21	0.22	0.23	0.36	0.26
Sc	10.55	19.59	21.01	22.00	21.56
V	13.60	154.54	158.25	211.06	159.67
Cr	0.00	71.21	98.26	44.12	75.11
Co	0.21	7.44	10.77	21.52	6.81
Ni	36.18	56.91	82.38	67.79	44.86
Pb	31.35	7.93	9.50	11.32	7.77
Cs	3.12	8.35	11.81	4.98	8.96
La/Th	1.99	1.72	1.65	2.49	1.84
Th/Yb	3.90	4.77	6.40	1.91	3.82
Th/Sc	0.53	0.36	0.47	0.21	0.31
Th/U	0.82	6.75	6.59	1.66	6.35
Sm/Nd	0.23	0.20	0.19	0.25	0.21
Eu/Eu*	0.70	0.91	0.81	0.83	0.89
⁸⁷ Sr/ ⁸⁶ Sr	0.70947	0.70889	0.71132	0.70758	0.70861
¹⁴³ Nd/ ¹⁴⁴ Nd	0.512353	0.512361	0.512286	0.512521	0.512367
ε _{Nd} (0)	-5.6	-5.4	-6.9	-2.3	-5.3
T _{DM} (Ga)	1.39	1.15	1.16	1.30	1.20

Table 4.5: Continued

Sample code	SL-11 (115-120)	SL-12 (125-130)	SL-13 (135-140)	SL-14 (145-150)	SL-15 (155-160)
Mean Depth (cm)	117.5	127.5	137.5	147.5	157.5
<i>(wt. %)</i>					
SiO ₂	62.66	61.96	61.88		61.56
TiO ₂	0.83	0.95	0.86		0.89
Al ₂ O ₃	18.46	19.27	19.89		19.27
Fe ₂ O ₃ ^T	5.85	9.18	8.17		8.71
MnO	0.04	0.06	0.06		0.06
MgO	3.09	3.03	3.20		2.91
CaO	3.55	2.06	2.23		2.10
Na ₂ O	3.64	1.13	1.50		1.48
K ₂ O	1.83	2.27	2.16		2.25
P ₂ O ₅	0.04	0.07	0.05		0.77
CIA	67.16	77.93	77.16		76.78
K ₂ O/Na ₂ O	0.50	2.00	1.44		1.51
<i>(ppm)</i>					
Rb	122.95	129.65	140.85	131.36	115.66
Sr	70.63	56.01	60.59	69.60	213.64
Ba	291.39	258.92	381.89	376.87	340.36
Y	8.46	8.46	9.19	11.04	20.19
Zr	63.80	59.10	76.76	62.36	41.44
Hf	2.11	2.09	2.20	2.01	1.86
Nb	6.78	6.84	7.48	6.60	6.24
Ta	0.48	0.48	0.51	0.49	0.51
Th	9.09	10.74	10.63	10.42	12.58
U	1.22	1.79	1.60	2.03	8.02
La	15.51	17.65	17.58	18.25	26.93
Ce	29.82	33.93	33.64	36.52	59.09
Pr	3.45	3.93	3.89	4.20	6.77
Nd	12.53	14.28	14.14	15.52	26.02
Sm	2.33	2.58	2.52	2.99	5.64
Eu	0.63	0.64	0.60	0.74	1.32
Gd	2.11	2.33	2.24	2.73	5.47
Tb	0.29	0.30	0.30	0.36	0.73
Dy	1.88	1.97	1.83	2.32	4.52
Ho	0.39	0.40	0.39	0.48	0.83
Er	1.33	1.34	1.30	1.53	2.49
Tm	0.19	0.19	0.19	0.21	0.33
Yb	1.39	1.43	1.41	1.55	2.35
Lu	0.20	0.21	0.20	0.23	0.35
Sc	16.44	18.19	21.48	20.75	13.13
V	122.18	129.20	164.85	157.56	115.68
Cr	71.79	87.89	101.89	85.33	50.44
Co	2.14	11.79	12.28	15.18	12.28
Ni	38.11	76.32	94.60	92.32	97.04
Pb	9.14	11.56	10.21	11.54	40.59
Cs	12.16	12.55	13.65	12.61	11.83
La/Th	1.71	1.64	1.65	1.75	2.14
Th/Yb	6.52	7.52	7.52	6.73	5.36
Th/Sc	0.55	0.59	0.49	0.50	0.96
Th/U	7.46	5.99	6.63	5.14	1.57
Sm/Nd	0.19	0.18	0.18	0.19	0.22
Eu/Eu*	0.84	0.77	0.75	0.77	0.70
⁸⁷ Sr/ ⁸⁶ Sr	0.71169	0.71222	0.71343	0.71155	0.71088
¹⁴³ Nd/ ¹⁴⁴ Nd	0.512241	0.512197	0.512184	0.512258	0.512267
$\epsilon_{Nd}(0)$	-7.7	-8.6	-8.9	-7.4	-7.2
T_{DM} (Ga)	1.21	1.24	1.24	1.23	1.42

Table 4.5: Continued

Sample code	SL-33 (165-170)	SL-16 (175-180)	SL-17 (195-200)	SL-18 (210-215)	SL-19 (225-230)
Mean Depth (cm)	167.5	177.5	197.5	212.5	227.5
(wt. %)					
SiO ₂	62.77	61.63	63.78	57.01	54.01
TiO ₂	0.97	0.89	0.95	0.77	0.71
Al ₂ O ₃	19.86	19.44	18.90	17.81	16.78
Fe ₂ O ₃ ^T	8.18	8.67	8.49	8.00	7.59
MnO	0.06	0.06	0.05	0.06	0.18
MgO	2.73	3.10	2.44	2.86	2.83
CaO	2.01	2.15	1.52	2.01	2.62
Na ₂ O	1.10	1.52	1.10	8.51	8.02
K ₂ O	2.24	2.38	2.25	2.38	2.60
P ₂ O ₅	0.06	0.16	0.53	0.59	4.68
CIA	78.78	76.26	79.51	58.00	55.91
K ₂ O/Na ₂ O	2.03	1.56	2.04	0.28	0.32
(ppm)					
Rb		148.29	139.52	141.35	168.18
Sr		69.86	64.86	184.53	26.00
Ba		351.04	310.22	270.50	307.88
Y		8.55	5.55	16.50	9.73
Zr		62.77	48.64	31.75	57.13
Hf		2.38	1.98	1.62	2.39
Nb		8.36	8.54	7.16	9.03
Ta		0.60	0.66	0.52	0.63
Th		11.26	9.54	13.58	12.70
U		1.91	1.33	4.62	2.46
La		19.42	18.94	28.02	23.61
Ce		37.93	37.18	62.78	47.75
Pr		4.45	4.40	6.80	5.52
Nd		16.42	16.18	25.85	20.25
Sm		3.01	3.00	5.40	3.81
Eu		0.74	0.71	1.24	0.86
Gd		2.71	2.57	5.12	3.35
Tb		0.34	0.31	0.67	0.43
Dy		2.20	1.91	3.97	2.63
Ho		0.44	0.36	0.71	0.52
Er		1.46	1.10	2.13	1.64
Tm		0.21	0.16	0.27	0.24
Yb		1.49	1.10	1.98	1.71
Lu		0.21	0.15	0.28	0.25
Sc		18.55	17.28	13.80	18.19
V		143.00	128.51	130.93	120.05
Cr		89.22	89.56	76.75	121.75
Co		11.14	4.21	18.25	14.86
Ni		91.33	64.63	118.11	122.52
Pb		8.85	7.20	39.59	11.66
Cs		14.65	12.41	14.65	16.44
La/Th		1.73	1.99	2.06	1.86
Th/Yb		7.54	8.70	6.87	7.43
Th/Sc		0.61	0.55	0.98	0.70
Th/U		5.90	7.16	2.94	5.17
Sm/Nd		0.18	0.19	0.21	0.19
Eu/Eu*		0.77	0.76	0.70	0.71
⁸⁷ Sr/ ⁸⁶ Sr	0.71135	0.71349	0.71299	0.71140	0.71680
¹⁴³ Nd/ ¹⁴⁴ Nd	0.512265	0.512204	0.512210	0.512321	0.512206
ε _{Nd} (0)	-7.3	-8.5	-8.3	-6.2	-8.4
T _{DM} (Ga)		1.25	1.25	1.26	1.28

Table 4.5: Continued

Sample code	SL-20 (240-245)	SL-21 (255-260)	SL-34 (265-270)	SL-22 (275-280)	SL-23 (285-290)
Mean Depth (cm)	242.5	257.5	267.5	277.5	287.5
(wt. %)					
SiO ₂	60.61	59.37	58.25	62.40	57.76
TiO ₂	0.87	0.86	0.93	0.91	0.76
Al ₂ O ₃	18.41	17.96	18.17	19.11	17.21
Fe ₂ O ₃ ^T	8.73	8.16	8.77	6.74	6.02
MnO	0.07	0.09	0.06	0.08	0.09
MgO	3.36	3.25	2.86	3.19	3.16
CaO	2.14	3.76	0.82	1.96	5.29
Na ₂ O	3.10	2.93	7.73	2.20	7.71
K ₂ O	2.07	1.97	2.34	2.37	1.90
P ₂ O ₅	0.64	1.66	0.06	1.01	0.09
CIA	71.58	67.47	62.52	74.51	53.60
K ₂ O/Na ₂ O	0.67	0.67	0.30	1.08	0.25
(ppm)					
Rb	139.50	48.52		104.46	121.79
Sr	51.67	366.31		141.60	103.36
Ba	344.96	139.44		200.82	330.29
Y	8.77	35.61		16.80	12.41
Zr	61.86	21.00		39.09	85.22
Hf	2.24	1.37		2.00	2.68
Nb	8.24	3.44		6.23	7.68
Ta	0.60	0.29		0.44	0.53
Th	9.98	18.37		11.26	9.51
U	1.60	5.91		4.70	1.55
La	19.64	36.12		23.71	18.18
Ce	38.74	94.25		55.66	37.08
Pr	4.59	9.60		5.94	4.43
Nd	16.96	38.43		23.11	16.77
Sm	3.17	9.12		5.03	3.35
Eu	0.79	2.18		1.19	0.88
Gd	2.82	9.31		4.89	3.09
Tb	0.36	1.32		0.68	0.42
Dy	2.28	8.13		4.19	2.74
Ho	0.45	1.45		0.77	0.55
Er	1.49	4.26		2.31	1.77
Tm	0.21	0.55		0.31	0.24
Yb	1.53	3.74		2.22	1.78
Lu	0.22	0.54		0.32	0.26
Sc	18.73	11.06		12.47	20.39
V	134.16	23.78		103.58	160.63
Cr	118.29	-0.09		52.20	120.64
Co	10.63	3.32		15.40	20.54
Ni	103.44	59.51		113.88	116.20
Pb	7.07	32.68		33.48	9.47
Cs	12.68	5.35		10.71	10.98
La/Th	1.97	1.97		2.11	1.91
Th/Yb	6.54	4.91		5.08	5.35
Th/Sc	0.53	1.66		0.90	0.47
Th/U	6.22	3.11		2.40	6.13
Sm/Nd	0.19	0.24		0.22	0.20
Eu/Eu*	0.78	0.70		0.71	0.81
⁸⁷ Sr/ ⁸⁶ Sr	0.71317	0.70954	0.71753	0.71069	0.71073
¹⁴³ Nd/ ¹⁴⁴ Nd	0.512243	0.512226	0.512214	0.512279	0.512311
ε _{Nd} (0)	-7.7	-8.0	-8.3	-7.0	-6.4
T _{DM} (Ga)	1.22	1.72		1.40	1.21

Table 4.5: Continued

Sample code	SL-24 (295-300)	SL-35 (305-310)	SL-25 (315-320)	SL-26 (325-330)	SL-27 (340-345)
Mean Depth (cm)	297.5	307.5	317.5	327.5	342.5
(wt. %)					
SiO ₂	61.10		64.87	61.41	63.28
TiO ₂	0.86		0.94	0.76	0.91
Al ₂ O ₃	19.08		20.10	17.65	19.79
Fe ₂ O ₃ ^T	6.97		5.64	7.16	7.68
MnO	0.08		0.04	0.04	0.04
MgO	3.56		2.84	3.45	2.96
CaO	2.75		1.08	3.80	1.48
Na ₂ O	2.63		1.35	2.86	1.08
K ₂ O	2.35		2.58	2.29	2.63
P ₂ O ₅	0.64		0.54	0.58	0.13
CIA	71.18		80.04	66.36	79.22
K ₂ O/Na ₂ O	0.89		1.90	0.80	2.44
(ppm)					
Rb	103.42		95.63	153.47	130.39
Sr	49.66		201.42	75.05	301.62
Ba	253.76		201.24	328.61	364.38
Y	6.64		20.33	9.59	18.85
Zr	46.38		36.05	59.64	57.39
Hf	1.66		1.37	1.91	2.05
Nb	6.75		5.15	8.79	6.48
Ta	0.46		0.39	0.81	0.48
Th	7.66		12.23	11.70	13.26
U	1.13		3.52	1.66	9.71
La	15.17		25.42	19.64	26.98
Ce	30.22		58.75	38.08	57.59
Pr	3.56		6.31	4.44	6.56
Nd	13.29		24.20	15.79	24.75
Sm	2.51		5.23	2.86	5.09
Eu	0.61		1.16	0.64	1.16
Gd	2.21		5.09	2.49	4.79
Tb	0.28		0.69	0.32	0.65
Dy	1.79		4.20	1.98	4.00
Ho	0.33		0.77	0.39	0.78
Er	1.03		2.32	1.29	2.35
Tm	0.15		0.31	0.18	0.32
Yb	1.06		2.11	1.37	2.31
Lu	0.15		0.31	0.19	0.33
Sc	14.44		13.28	16.57	15.29
V	101.89		106.97	130.74	140.71
Cr	82.48		59.08	111.04	80.01
Co	13.22		14.27	10.76	13.79
Ni	80.70		79.45	83.85	112.53
Pb	6.18		35.99	8.51	46.16
Cs	9.22		9.60	13.76	13.56
La/Th	1.98		2.08	1.68	2.04
Th/Yb	7.24		5.79	8.55	5.74
Th/Sc	0.53		0.92	0.71	0.87
Th/U	6.80		3.48	7.05	1.37
Sm/Nd	0.19		0.22	0.18	0.21
Eu/Eu*	0.77		0.66	0.71	0.70
⁸⁷ Sr/ ⁸⁶ Sr	0.71466	0.71330	0.71063	0.71186	0.71071
¹⁴³ Nd/ ¹⁴⁴ Nd	0.512205	0.512252	0.512136	0.512175	0.512225
ε _{Nd} (0)	-8.4	-7.5	-9.8	-9.0	-8.1
T _{DM} (Ga)	1.28		1.63	1.27	1.39

Table 4.5: Continued

Sample code	SL-36 (355-360)	SL-28 (365-370)	SL-29 (375-380)	SL-30 (385-390)	SL-31 (395-400)
Mean Depth (cm)	357.5	367.5	377.5	387.5	397.5
(wt. %)					
SiO ₂	65.17		61.76	62.44	
TiO ₂	0.96		0.89	0.90	
Al ₂ O ₃	20.21		18.81	19.13	
Fe ₂ O ₃ ^T	5.75		7.67	7.12	
MnO	0.05		0.07	0.07	
MgO	2.57		3.21	3.14	
CaO	1.48		3.68	2.77	
Na ₂ O	1.12		1.72	1.42	
K ₂ O	2.52		2.12	2.17	
P ₂ O ₅	0.16		0.10	0.86	
CIA	79.79		71.44	75.04	
K ₂ O/Na ₂ O	2.24		1.23	1.53	
(ppm)					
Rb	136.30		113.92	128.04	120.46
Sr	72.95		111.74	93.13	112.06
Ba	274.06		319.53	287.90	508.28
Y	9.91		15.08	11.68	13.46
Zr	109.16		93.69	73.49	75.88
Hf	2.92		2.46	2.26	2.26
Nb	8.82		7.04	7.85	7.64
Ta	0.63		0.58	0.54	0.54
Th	9.30		8.44	8.90	9.45
U	1.56		1.36	1.41	2.05
La	19.12		16.05	18.39	19.78
Ce	36.90		32.09	36.05	39.77
Pr	4.29		3.82	4.24	4.67
Nd	15.62		14.33	15.60	17.42
Sm	2.77		2.79	2.93	3.38
Eu	0.66		0.74	0.73	0.85
Gd	2.40		2.70	2.64	3.15
Tb	0.30		0.38	0.35	0.42
Dy	2.02		2.56	2.27	2.67
Ho	0.42		0.53	0.47	0.52
Er	1.41		1.78	1.54	1.69
Tm	0.20		0.25	0.22	0.24
Yb	1.45		1.77	1.58	1.76
Lu	0.21		0.27	0.23	0.26
Sc	18.65		23.31	20.83	20.13
V	144.38		205.05	153.32	149.79
Cr	116.70		132.94	119.87	126.60
Co	8.79		13.76	12.11	18.29
Ni	77.91		87.27	87.00	116.97
Pb	7.87		6.95	8.47	17.78
Cs	12.65		10.31	12.03	11.19
La/Th	2.06		1.90	2.07	2.09
Th/Yb	6.42		4.76	5.63	5.37
Th/Sc	0.50		0.36	0.43	0.47
Th/U	5.97		6.22	6.31	4.61
Sm/Nd	0.18		0.19	0.19	0.19
Eu/Eu*	0.76		0.80	0.78	0.77
⁸⁷ Sr/ ⁸⁶ Sr	0.71048	0.71155	0.71436	0.71644	0.71132
¹⁴³ Nd/ ¹⁴⁴ Nd	0.512203	0.512280	0.512352	0.512279	0.512279
ε _{Nd} (0)	-8.5	-7.0	-5.6	-7.0	-7.0
T _{DM} (Ga)	1.21		1.11	1.17	1.22

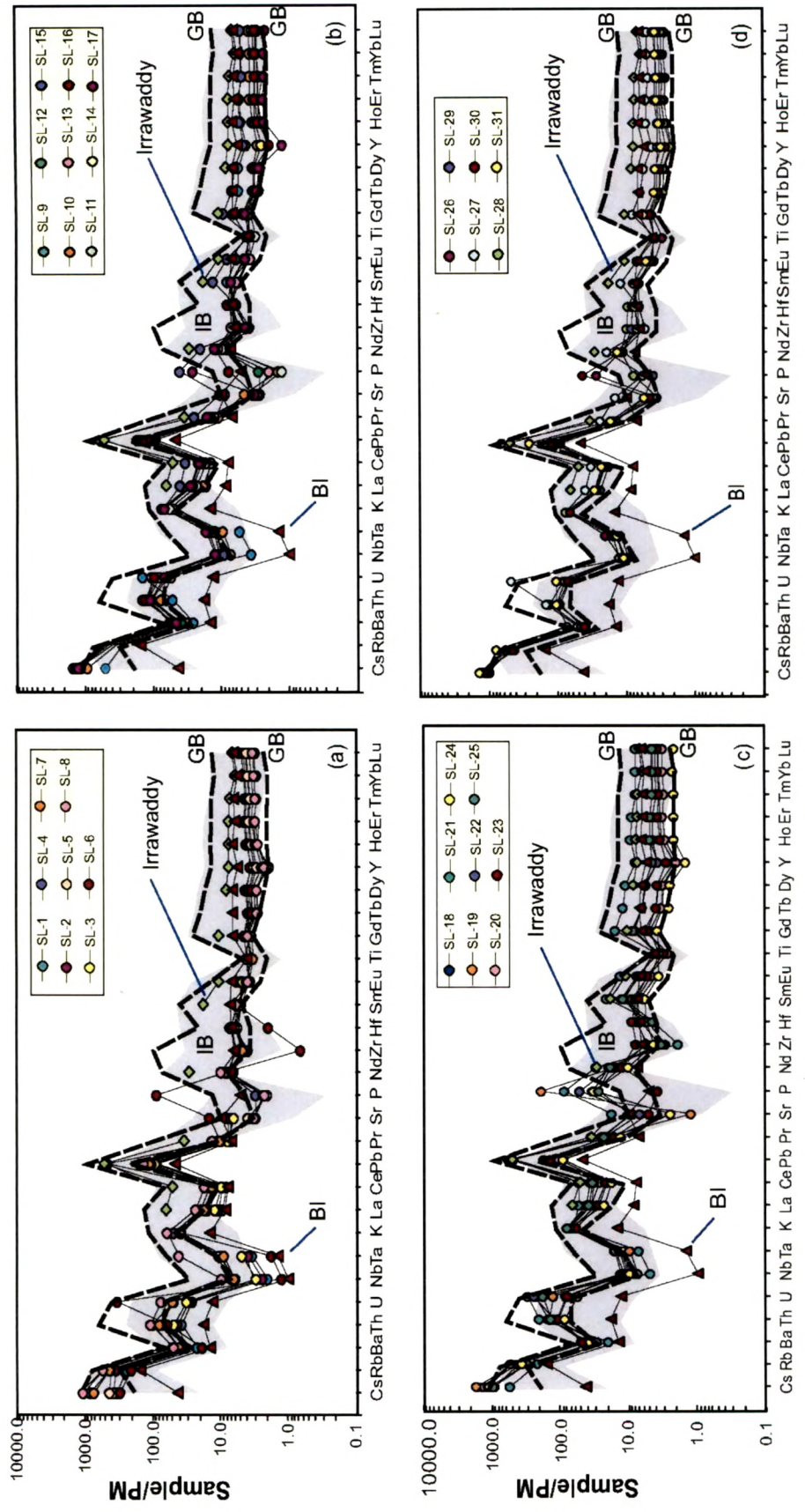


Fig. 4.16: Primitive mantle (PM) normalized multi element spidergrams for the sediments in the core. Data Sources: average compositions of Irrawaddy sediments (Kurian et al., 2008); Barren Island volcanic (BI) (Luhr and Haldar, 2006; Pal et al., 2010); fields for sediments from Indo-Burman (IB) sources (this study, determined from rocks of Andaman Islands); sediments from Himalayan sources brought by Ganga-Brahmaputra (GB, dashed line) (Stummeyer et al., 2002).

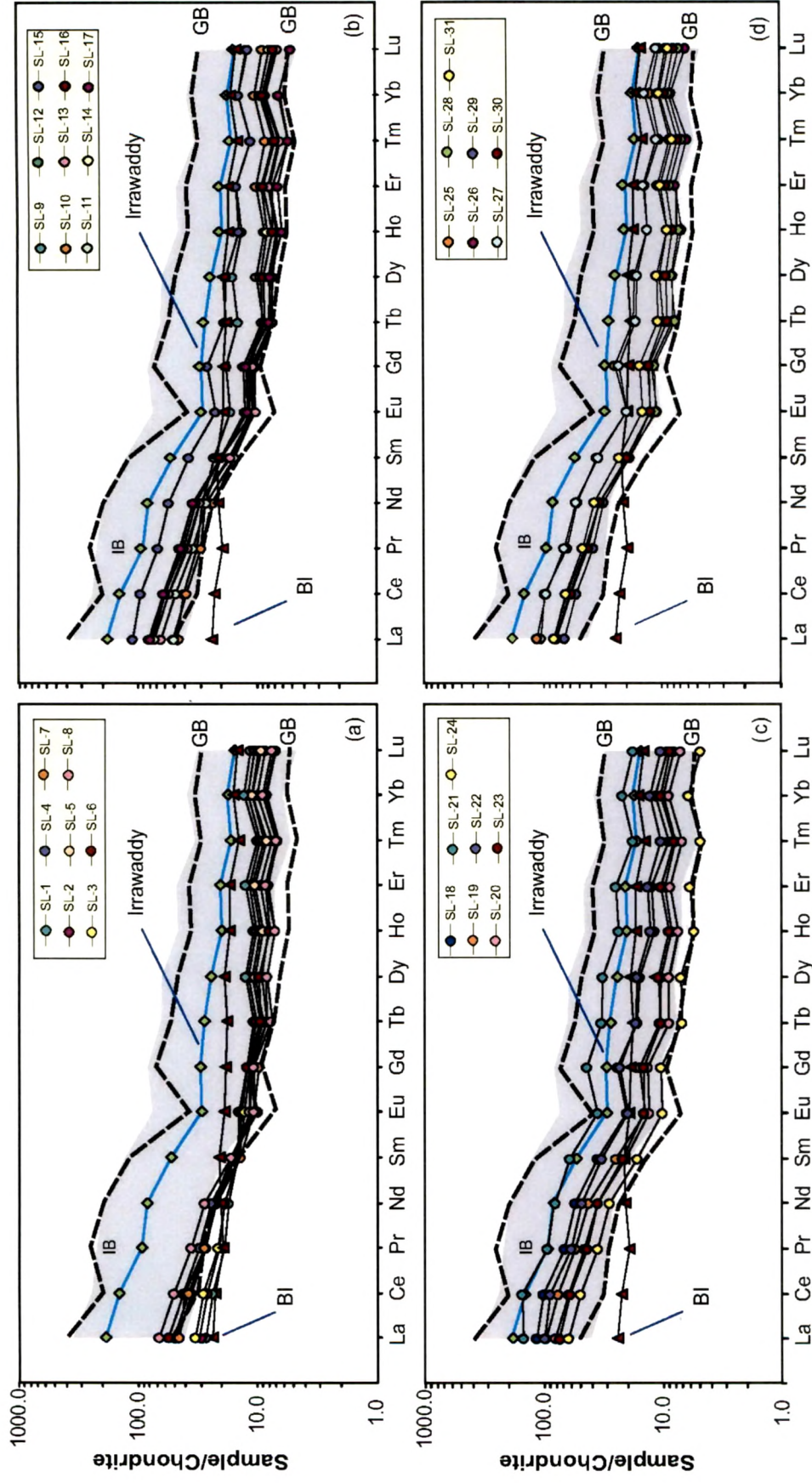
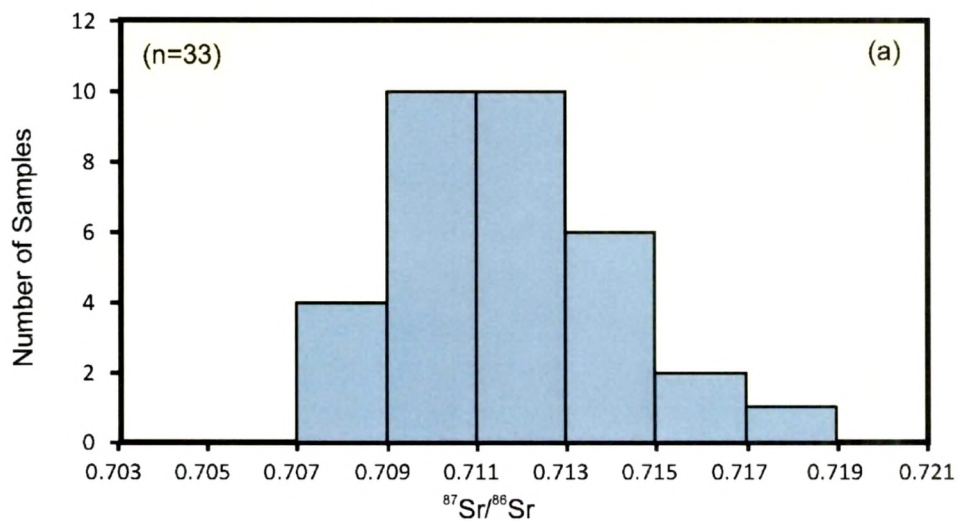


Fig. 4.17: Chondrite normalized REE patterns for the sediments in the core. Fields are same as in Fig. 4.16.

6. The chondrite-normalized REE patterns for sediment layers in the core show enriched light REE patterns (Fig. 4.17), which tend to become more enriched towards the older half of the core (Fig. 4.17a-d). The total LREE contents in the top layers are much lower than that in the rest and in the sediments of the Irrawaddy and G-B river systems (Fig. 4.17a). The HREE patterns are relatively flat and all layers show moderate negative Eu anomalies ($\text{Eu}/\text{Eu}^* = 0.7\text{-}1.1$).
7. In both the plots, Fig. 4.16 and Fig. 4.17, the trace element contents in the sediments from the core overlap with the fields drawn for the Indo-Burman (IB) and Himalayan sources.

(C) Sr-Nd Isotopic ratios

Sr-Nd isotopic ratio analyses were also carried out on the decarbonated siliclastic sediments from selected layers in the core. These data are presented in Table 4.5 and in histograms in Fig. 4.18. Neglecting the top disturbed part of the core, the data reveal that $^{87}\text{Sr}/^{86}\text{Sr}$ of sediments varies between 0.707 and 0.718 and ϵ_{Nd} values range from -9.8 to -2.3. The modes of $^{87}\text{Sr}/^{86}\text{Sr}$ and ϵ_{Nd} distributions in our core are 0.711 and -7, respectively (Fig. 4.18a and b). The lower part of the core between 120 cm and 400 cm, contains more radiogenic Sr (and non-radiogenic Nd) bearing sediments, while sediments from top 120 cm of the core have comparatively lower $^{87}\text{Sr}/^{86}\text{Sr}$ and higher ϵ_{Nd} . The lowest $^{87}\text{Sr}/^{86}\text{Sr}$ value (and the highest ϵ_{Nd} value) is observed at ~100 cm depth.



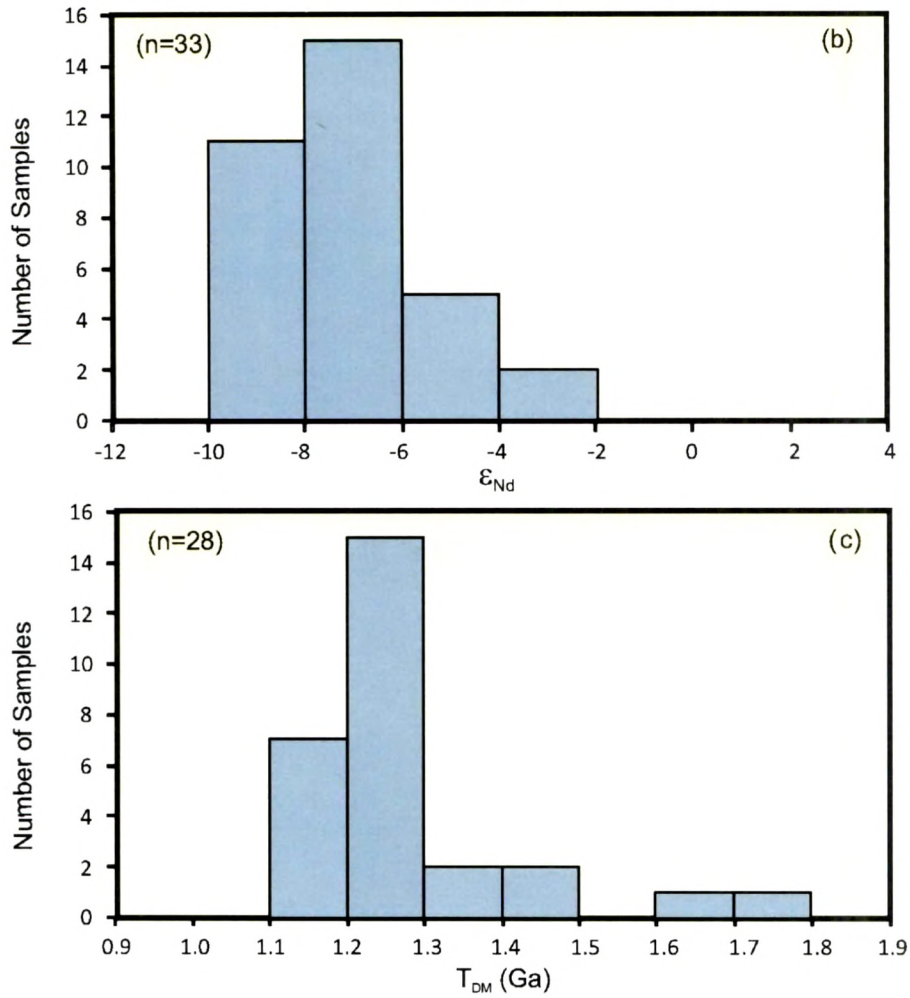


Fig. 4.18: Histograms showing frequency distributions of (a) $^{87}\text{Sr}/^{86}\text{Sr}$, (b) ϵ_{Nd} and (c) TDM ages for siliciclastic sediment layers in the core SK-234-60.

The ϵ_{Nd} versus $^{87}\text{Sr}/^{86}\text{Sr}$ compositions of core sediments are plotted in Fig. 4.21. Overall, our data show values with lower $^{87}\text{Sr}/^{86}\text{Sr}$ and higher ϵ_{Nd} as compared to the studies done on sediments from the other parts of the Andaman Sea (Colin et al., 1999). The histogram for the depleted mantle ages (T_{DM}) for these sediments is shown in Fig. 4.18c. The T_{DM} ages range from 1.11 Ga to 1.72 Ga and show a prominent mode at ~ 1.25 Ga (Fig. 4.18c).

4.5.3 Discussion

(A) Weathering in the source regions

Chemical Index of Alteration (CIA) and $\text{Al}_2\text{O}_3 + (\text{CaO}^* + \text{Na}_2\text{O}) + \text{K}_2\text{O}$ (A-CN-K) ternary diagram provide valuable information about the weathering conditions at the

sources at the time of derivation of these sediments in our core. Figure 4.19 shows our data plotted in an A–CN–K diagram with CIA scale on the left. Our data points trend parallel to the A–CN join suggesting variable degree of weathering of source rocks. The CIA value of these sediments varies from 53 to 80, which again hint at low to moderate degree of weathering of their sources. The sources for the sediments are compositionally similar to tonalities suggesting higher contribution from lower crust and/or juvenile mafic igneous rocks compared to sediments in Bay of Bengal or to PAAS. We suspect that this juvenile material contribution could have come from the Indo-Burman mountain ranges of Myanmar.

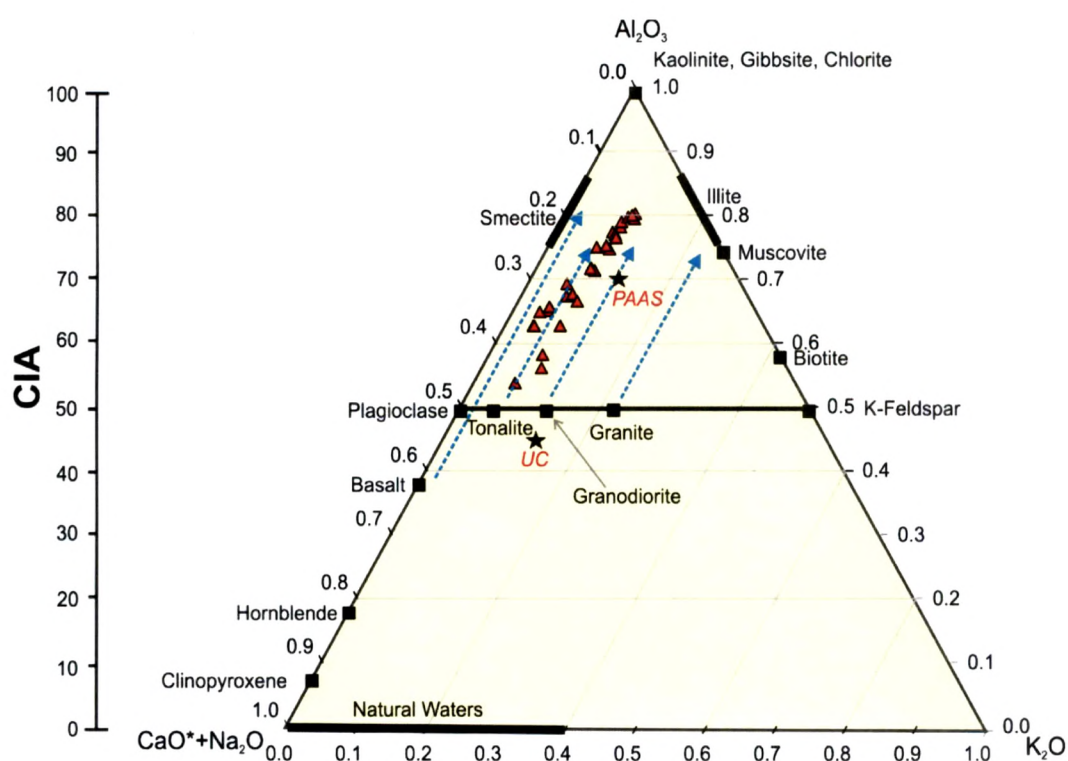


Fig. 4.19: A–CN–K diagram with the Chemical Index of Alteration (CIA) of Nesbitt et al, (1996) on which core sediments are plotted. Also shown on the diagram are the positions of minerals, post-Archean Australian Average Shale (PAAS), and average Archean upper crust. Arrows emanating from plagioclase–K-feldspar join show the weathering trends for basalt, tonalite, granodiorite and granite (Nesbitt and Young, 1984, 1989).

Th/U ratios in sediments are controlled by weathering-erosion-diagenesis cycle (Condie, 1993). In Fig. 4.20, Th/U ratios of most of our samples are higher than the upper crustal value of 3.8 (Taylor and McLennan, 1985) suggesting derivation from

recycled crustal material, which has lost U. Two of our samples plot within the field for depleted mantle indicating their link to magmatic arc volcanoes. Some samples show lower Th/U ratios and higher Th values. These samples probably suffered U enrichment under reducing conditions of deposition.

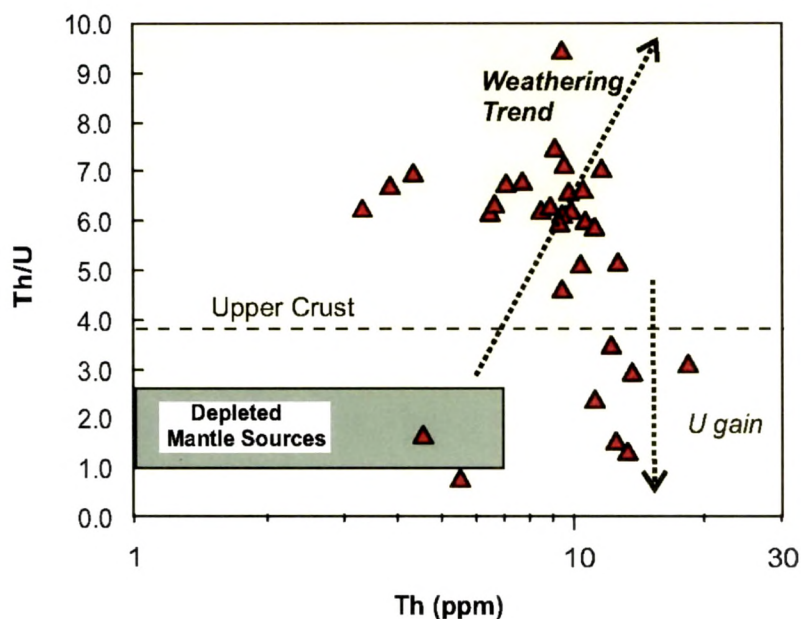


Fig. 4.20: Plot of Th/U versus Th (after McLennan et al., 1995) for the core sediment samples from the core.

(B) Provenance

Significant variations observed in the Sr and Nd isotopic compositions of the sediments probably indicate variable contributions from multiple sources to the core site. In the absence of Sr-Nd isotopic data on likely continental sources, we used published data on sediments from major river systems that drain into the Bay of Bengal and Andaman Sea and compared them with our data. As suggested by earlier studies, the main source of sediments to the Andaman Sea is the sediments discharged by the Irrawaddy river system (Colin et al., 1999; Ramaswamy et al., 2004). However, considering that there exists a major easterly flowing surface current during the period of South-West monsoon (Rodolfo, 1969), we expect significant sediment contribution of Himalayan derived Ganga-Brahmaputra (G-B) sediments from the Bay of Bengal to the Andaman Sea by this current. Comparing $^{87}\text{Sr}/^{86}\text{Sr}$ and ϵ_{Nd} data from our core (SK-234), with the available data from other cores studied in the Andaman Sea and NE Bay of Bengal

(Fig. 4.21), we observe that isotopic ratios in our core ($^{87}\text{Sr}/^{86}\text{Sr}= 0.707\text{--}0.718$; $\epsilon_{\text{Nd}}= -9.8$ to -2.3) are less radiogenic as compared to the sediments of the eastern Andaman Sea ($^{87}\text{Sr}/^{86}\text{Sr}= 0.712$ to 0.719 ; $\epsilon_{\text{Nd}}= -10.8$ to -9.3 , Core-MD77-169, Colin et al., 2006) and sediments from Irrawaddy ($^{87}\text{Sr}/^{86}\text{Sr}= 0.713$; $\epsilon_{\text{Nd}}= -10.7$, Colin et al., 1999) (Fig. 4.21). This observation points to the involvement of sources other than Irrawaddy which were also actively supplying sediments to the core site (Fig. 4.15). While most of the isotopic data from our core overlap with those from the cores MD77-171 and MD77-176, a general shift towards lower $^{87}\text{Sr}/^{86}\text{Sr}$ and higher ϵ_{Nd} values is observed. Such a trend appears to be a result of contributions from a third source. We believe that Cretaceous-Oligocene sedimentary rocks, volcanics and ophiolitic rocks present in the Indo-Burman Ranges (Allen et al., 2008; Colin et al., 2006) represent this third source.

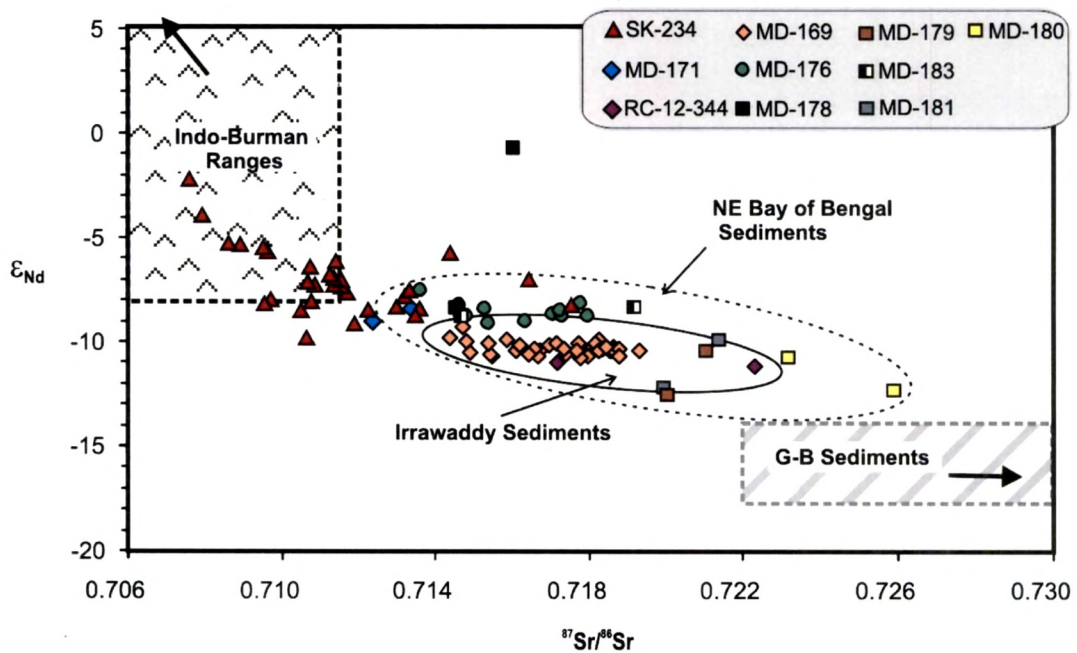


Fig. 4.21: Plot of ϵ_{Nd} versus $^{87}\text{Sr}/^{86}\text{Sr}$ for sediments from our core (SK-234) and cores in the region studied by others. Data sources: sediments of Irrawaddy, sediments of the cores from Andaman Sea and NE-Bay of Bengal: Colin et al., (1999), Colin et al., (2006); Indo-Burman Ranges: Allen et al., (2008), this study, determined from rocks of Andaman Islands; Ganga-Brahmaputra (G-B): Ahmad et al., (2005) and references therein. All data were normalized to NBS-987 (0.710250) and La Jolla (0.511858) for $^{87}\text{Sr}/^{86}\text{Sr}$ and $^{143}\text{Nd}/^{144}\text{Nd}$ isotopic ratios, respectively.

From the above discussion it is apparent that our site received sediments from three different sources drainage systems; viz: Myanmar continental sediments through Irrawaddy river system, Indo-Burman mountain ranges and Himalaya derived Ganga-

Brahmaputra (G-B) sediments from the Bay of Bengal. A three component-mixing calculation using these three sources suggest that the Irrawaddy and Indo-Burman ranges are the main contributors of sediments to our core site; however, there has been significant contribution of G-B sediments from the north-east Bay of Bengal as well (Fig. 4.22). A closer look at these contributions through time reveals that the sediments deposited during the Last Glacial Maximum (LGM), with lower $^{87}\text{Sr}/^{86}\text{Sr}$ and high ϵ_{Nd} values, have relatively larger (upto 98 %) contribution from the Indo-Burman sources (Fig. 4.21 and 4.22).

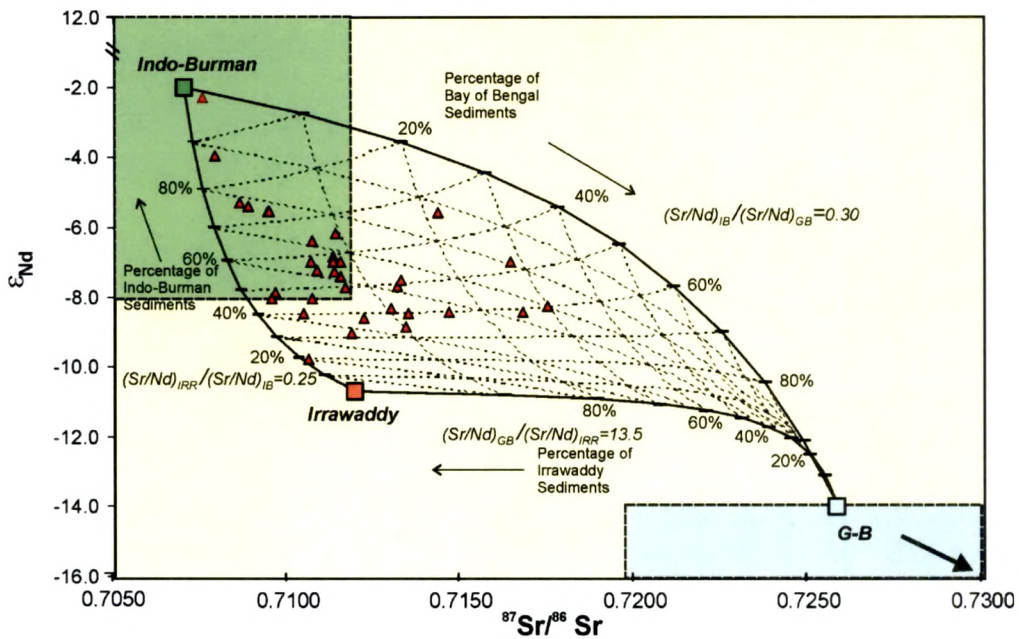


Fig. 4.22: Plot of ϵ_{Nd} vs. $^{87}\text{Sr}/^{86}\text{Sr}$ of sediments from our core compared with model curves of a three components mixing involving sediments from Indo-Burman Ranges, Irrawaddy river system and Ganga-Brahmaputra (G-B) river system. The end-member compositions used in these calculations are: Indo-Burman ($\text{Sr} = 200 \text{ ppm}$; $\text{Nd} = 24 \text{ ppm}$; $^{87}\text{Sr}/^{86}\text{Sr} = 0.707$; $\epsilon_{\text{Nd}} = -2$), Irrawaddy ($\text{Sr} = 100 \text{ ppm}$; $\text{Nd} = 50 \text{ ppm}$; $^{87}\text{Sr}/^{86}\text{Sr} = 0.712$; $\epsilon_{\text{Nd}} = -10.7$) and Ganga-Brahmaputra ($\text{Sr} = 400 \text{ ppm}$; $\text{Nd} = 15 \text{ ppm}$; $^{87}\text{Sr}/^{86}\text{Sr} = 0.726$; $\epsilon_{\text{Nd}} = -12.6$). The source for the end-member compositions are: Indo-Burman Ranges: Allen et al., (2008), this study, determined from rocks of Andaman Islands, Irrawaddy & G-B: Colin et al., (1999), Ahmad et al., (2005).

The results from isotopic data are further supported by the REE distributions in the samples from the core. The lower REE contents in these compared to that in Irrawaddy sediments suggest that there exists an additional source, possibly of mafic-magmatic in nature. As mentioned above such mafic sources, which can contribute sediments to the Andaman Sea, are extensively present only in Indo-Burman Ranges (Allen et al., 2008;

Colin et al., 2006). Except for the top disturbed part of the core (showing patterns similar to Barren Island volcano), all our data fall within the field drawn for the Indo-Burman sources (Fig. 4.17). Samples from further down the core show relatively enriched LREE pattern suggesting more contribution from felsic continental sources in the past (Fig. 4.17). These can be due to increased contribution from Himalyan derived sediments either carried through Irrawaddy or Ganga-Brahmaputra systems. Although the A-CN-K diagram (Fig. 4.19) suggests an average source rock composition for the core sediments to be tonalitic, considering the above results from isotopic ratios we believe that the evolutionary trend shown by core sediments reflects mixing of sediments from multiple sources (one basaltic and other granitic/granodioritic).

(C) Climatic Implications

The Sr-Nd isotopic ratios of sediments in the Andaman Sea show striking shift as a function of time (depth) (Fig. 4.23). These excursions apparently reflect changes in provenance and most likely are governed by changing monsoonal strength. In the following discussion we discuss climatic implications of the chemical variations observed in the core in three time periods: pre-LGM, during LGM and post-LGM. By doing so, we look into the sedimentary record to search for evidences for changes in the sea-level, oceanic circulation patterns, sediment transport and monsoonal intensity.

The down core record prior to the LGM (at 18 kyr) shows several excursions towards lower $^{87}\text{Sr}/^{86}\text{Sr}$ and higher ϵ_{Nd} at ~36 kyr, ~44 kyr, ~52 kyr and ~58 kyr (Fig. 4.23). We believe that these excursions, except for the ~52 kyr event, are correlated to the Heinrich events H4, H5 and H6, respectively, which occurred during the last glacial period (Hemming, 2004). The excursion at ~52 kyr might also be related to some event similar to it. Earlier studies have shown that during the Heinrich global cold events the intensity of the Asian summer monsoon had remained very weak (Porter and Zhisheng, 1995; Colin et al., 1998). The penetration of the monsoon in the interior parts of the continental source areas largely depends on its intensity. As rivers in South Asia are mainly fed by sediments eroded by rainfall during summer monsoons, the weak summer monsoons during these cold periods probably restricted the penetration of monsoonal rainfall into the inner parts of Myanmar and thus reducing the supply of high $^{87}\text{Sr}/^{86}\text{Sr}$ bearing sediments from the glaciated regions of the Himalaya.

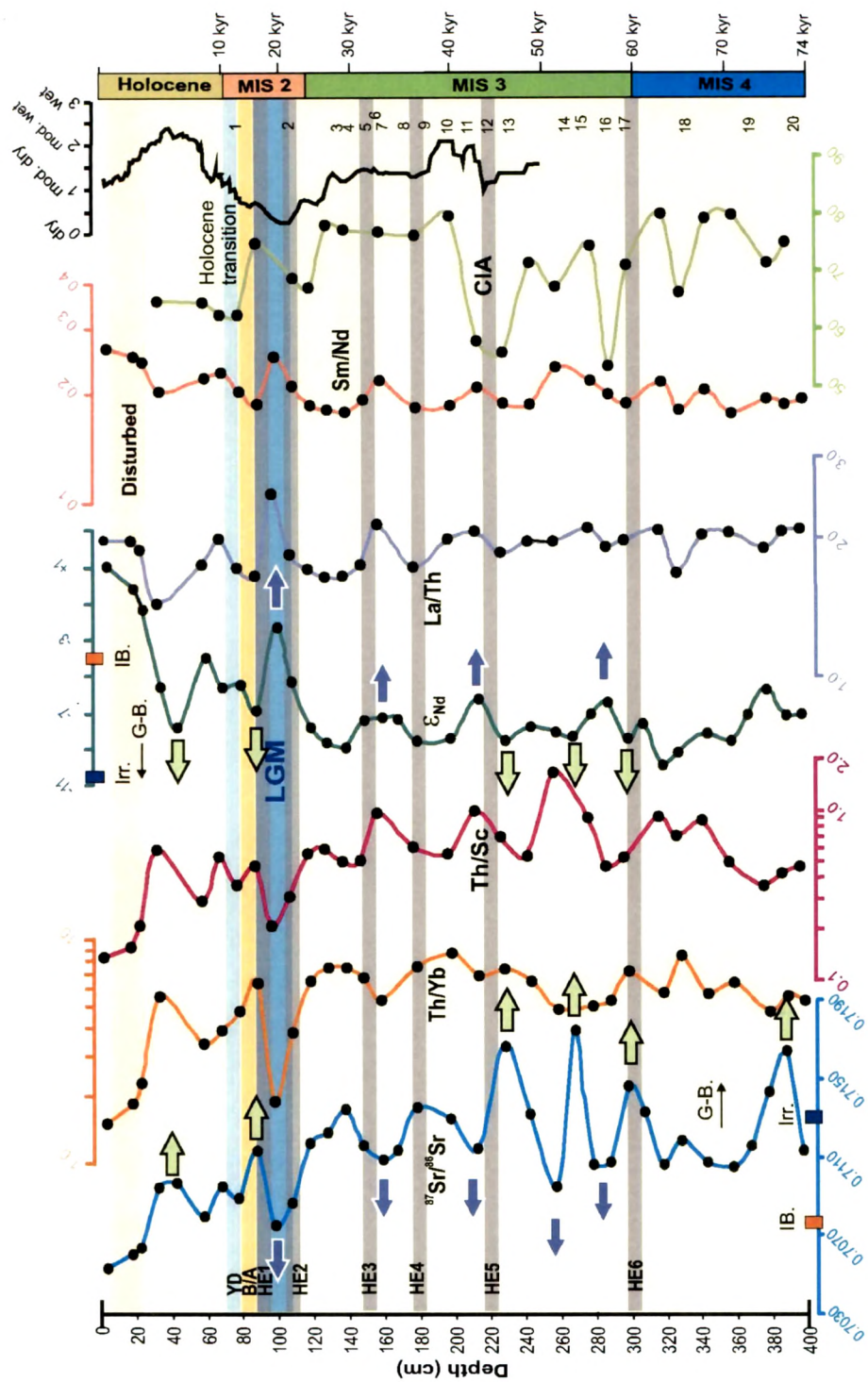


Fig. 4.23: Depth profiles of Sr-Nd isotopic compositions, trace element ratios and CIA values of sediments in our core SK-234-60. HE1-HE6 on left are Heinrich cold events (Hemming, 2004) and numbers 1 to 20 on right are Dansgaard-Oeschger warm events (Schulz, 2002). Curve for mean effective moisture is from Hershuh, (2006). The arrows mark significant excursions (purple: cold events and green warm events). Irr: Irrawaddy; IB: Indo-Burman Ranges; G-B: Ganga-Brahmaputra; MIS: Marine Isotopic Stage.

It is highly likely that during these events the relative contribution of sediments derived from the Indo-Burman Ranges, through the seaways between Bay of Bengal and Andaman Sea, increased to our core site. The weak summer monsoon conditions at ~36 kyr, ~47 kyr, and ~58 kyr BP have also been observed in a core studied from the Bay of Bengal by Colin et al. (1998), in which, increase in size of magnetic grains and decrease in CIA value have been correlated to Heinrich events. In our core, we also observe excursions in some key elemental ratios (La/Th, Th/Yb, Sm/Nd and Th/Sc) at the same places where isotopic shifts have been observed. These apparently are results of changes in provenance and relative contribution of sediments from felsic Himalayan-Transhimalayan sources and mafic Indo-Burman sources. The correlateable excursions observed in the isotopic data and geochemical indicators confirm that these variations are related to change in contribution of sediments from various sources, and not to processes like particle sorting/weathering (Colin et al., 2006; Tutken et al., 2002; Walter et al., 2000). As the sources are located in the inter-tropical regions, wet summer monsoons cause relative increase in chemical weathering of sediments in river plains, and loss of the most mobile elements (Na, K, and Ca) from the detrital minerals (feldspars and glass from volcanic rocks) producing pedogenic clays minerals (e.g., smectite; kaolinite) leading to increase in CIA value. In contrast, dry periods are characterized by enhanced physical erosion in the higher reaches which results in supply of high volumes of unaltered minerals that reduces the CIA value of bulk sediments. The lowering of CIA value in our core at ~44 kyr and ~ 58 kyr further support the hypothesis of weak summer monsoon conditions (related to Heinrich events) during these times. In addition to the above, we also observe variations that show significant increase in $^{87}\text{Sr}/^{86}\text{Sr}$ and decrease in ϵ_{Nd} at ~46 kyr, ~54 kyr, ~60 kyr and ~72 kyr in the core (Fig. 4.23). We postulate that these are associated with the Dansgaard-Oeschger warm events like DO-3, 8, 9, 10, 13 and 16 during which the South Asian summer monsoon had regained its strength that caused higher input from the Himalayan sources through Irrawaddy river system. Support for such an inference comes from an earlier study by Herzsuh (2006), which reported intensification of SW monsoon at ~47 ka and ~54 ka.

Many studies have shown that sediments discharged by the global rivers were greatly reduced during the LGM (Duplessy, 1982; Van Campo, 1986), when the sea level was

lower by 100-125 m (Chappell and Shackleton, 1986). Lower sedimentation rates during the LGM have also been reported from cores from the Bay of Bengal (Tripathy et al., 2011, Kessarkar et al., 2005, Galy et al., 2008). In fact, the lowest rate of the sedimentation observed by us in our core occurred during ~17-23.5 ka. This reduced supply of sediments to the Andaman Sea during the LGM could be attributed to slower continental erosion. The Sr-Nd isotopic composition observed in the core during the LGM support this hypothesis. The observed $^{87}\text{Sr}/^{86}\text{Sr}$ ratio during the LGM (~95–110 cm) is ~0.708 compared to its value of ~0.711 in sediments deposited before and after the LGM (Fig. 4.23). ϵ_{Nd} shows a higher value of -2.3 during the LGM compared to pre- and post-LGM values of -7 (Fig. 4.23). Similar trends of lower $^{87}\text{Sr}/^{86}\text{Sr}$ and higher ϵ_{Nd} during the LGM have also been observed in the sedimentary record of the Bay of Bengal (Tripathy et al., 2011). Such trends can be attributed to lowering of contribution from older continental sources particularly from the Himalayas. During the LGM mountain glaciers had covered much of the higher reaches of Tibet and Himalaya (Yokoyama, 2000; Tripathy et al., 2011) and there was a weak SW monsoon (Herzschuh, 2006; Prell and Kutzbach, 1987) and an intensified NE monsoon (Duplessy, 1982; Prell et al., 1980; Sarkar et al., 1990; Tiwari et al., 2005). It appears that the weakening of SW monsoonal rainfall is the primary reason for reduced erosion in the higher Himalayas and continental Myanmar which led to reduced sediment input from these sources. However, such a weakening probably did not affect the sediment derivation and input from the Indo-Burman Ranges, which explains the isotopic shifts. Such an inference is also supported by the work of Colin et al. (1999), who observed increase in ϵ_{Nd} during the LGM in cores from NE Bay of Bengal, known to have dominant contribution of sediments from the Indo-Burman Ranges. La/Th, Th/Sc, Sm/Nd and Th/Yb ratios of sediments in our core also show excursions at ~100 cm depth corresponding to the LGM indicating increase in contributions from mafic igneous sources (Fig. 4.23).

The sedimentary record subsequent to the LGM shows an increase in $^{87}\text{Sr}/^{86}\text{Sr}$ and decrease in ϵ_{Nd} at ~15 kyr, ~10 kyr and at ~6 kyr BP (Fig. 4.23). The first two excursions are probably related to events of intensification of the SW monsoon during warm and moist Bølling-Allerød (B/A) event that happened somewhere between 14.7

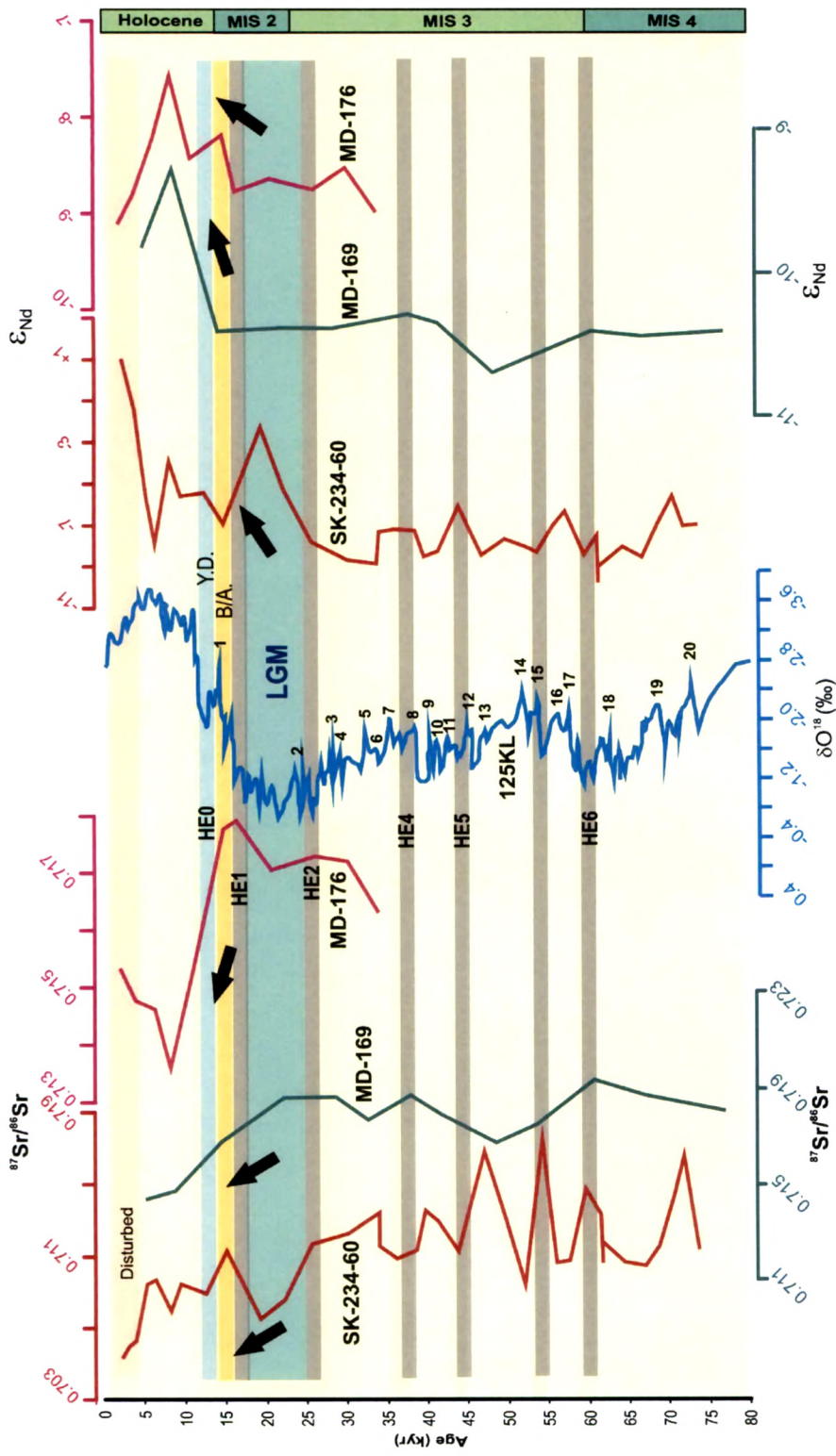


Fig. 4.24: Temporal variations of Sr and Nd isotopic compositions of sediments in core SK-234-60 compared with other cores MD77-169 (Sewell seamount), MD77-176 from the Andaman Sea. Also shown δO^{18} (‰) variations of core 125KL from Bay of Bengal (Kudrass et al., 2001). Numbers 1 to 20 are Dansgaard-Oeschger warm events while HE0-HE6 are Heinrich cold events (Hemming, 2004). YD: Younger Dryas event, B/A: Bølling-Allerød event, MIS: Marine Isotopic Stage.

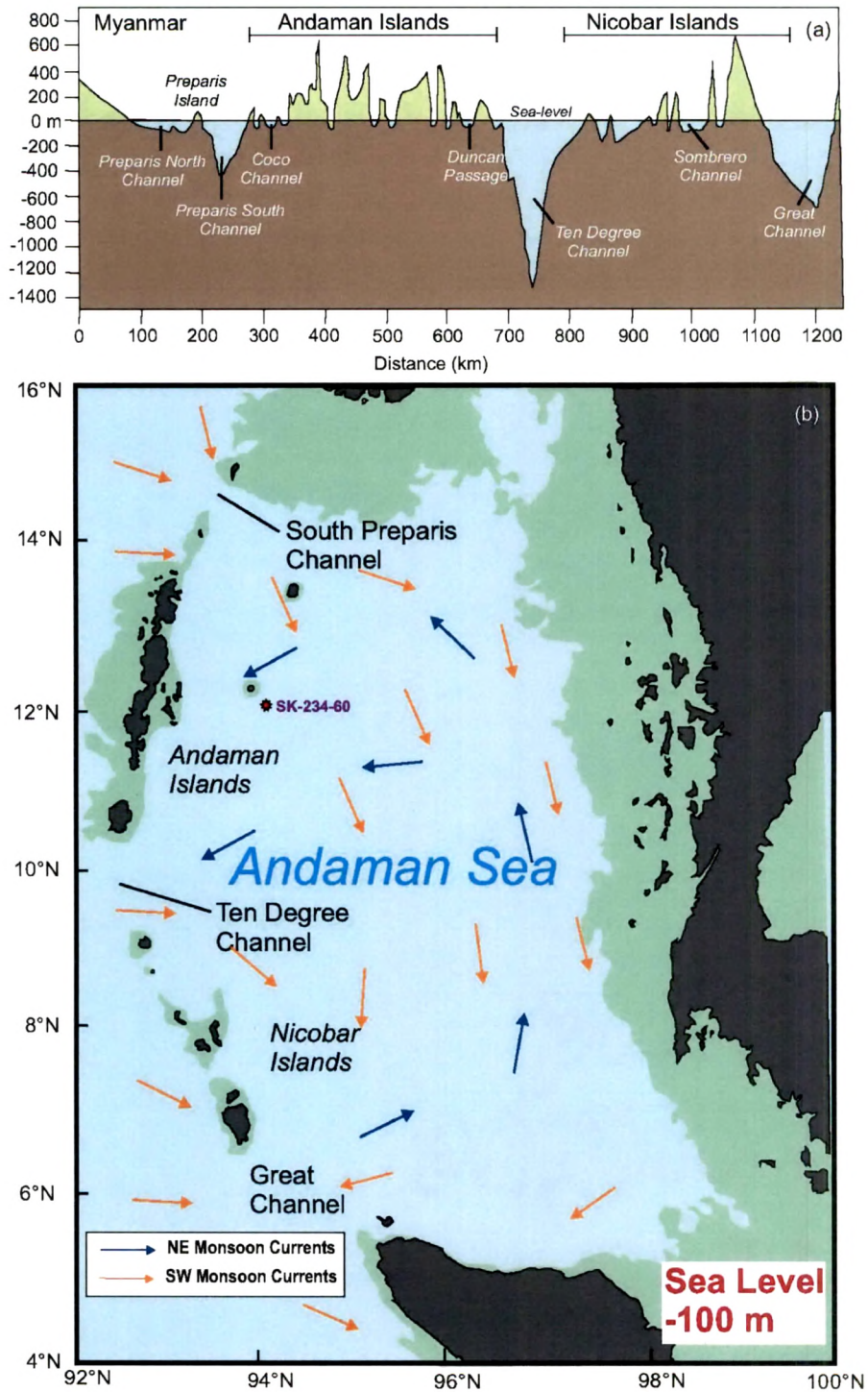


Fig. 4.25: (a) Present-day N-S bathymetric profile of Andaman and Nicobar ridge showing various channels through which Andaman Sea exchanges water with Bay of Bengal (b) The coastlines around the Andaman sea (shown in green shade) during the LGM with a 100m drop in sea-level. The South Preparis Channel was the only open passage between the Bay of Bengal and Andaman Sea then.

and 12.7 kyr (Cronin, 1999) and during the Pleistocene-Holocene transition (Bookhagen et al., 2005). The third excursion at ~6 kyr followed a weak summer monsoon event at ~8.2 kyr (Alley et al., 1997; Wang et al., 2005). The B/A event initiated the end of the cold period of the LGM and resulted in worldwide rise in the sea level to more than 100 m due to melting of glaciers. The excursions observed in $^{87}\text{Sr}/^{86}\text{Sr}$ and ϵ_{Nd} are correlatable to excursions seen in various elemental ratios and CIA (Fig. 4.23). The drop in CIA value at ~10 ka was probably due to sudden increase in supply of unweathered sediments during the Holocene transition. The chemical variations observed in the top 20 cm of the core have been neglected from discussion as it was disturbed and consisted of sediments mixed with inseparable volcanic ash.

(D) Implications for ocean circulation

For a better understanding of the provenance and climate signals in our core (SK-234-60), we compared our record with other such studies in the Andaman Sea and Bay of Bengal (Fig 4.22). The major climatic fluctuations observed in our core correlate well with that in the δO^{18} record in the core 125KL from the Bay of Bengal (Kudrass et al., 2001), which has been well correlated with major climatic variations in the northern hemisphere. The overall trend of deposition of non-radiogenic Sr (and radiogenic Nd) sediments in the core since the LGM suggests that mafic igneous sources, most likely located in the Indo-Burman Ranges, contributed significant amounts of sediments to the core site (Fig. 4.24). Similar trends, although with lower amplitudes, are also observed in several other cores from the Andaman Sea (e.g., MD77-176, MD77-169) (Fig. 4.24). We believe that these trends are related to the increase in the sea level after the LGM (Hashimi et al., 1995; Goodbred and Kuehl, 2000). During and before the LGM, the continental margins surrounding the Andaman Sea and Bay of Bengal consisted of exposed uplands and rivers such as Ganga, Brahmaputra, Irrawaddy and Salween incised into the continental shelf- pouring sediments directly into the deep sea. The low sea level must have influenced the water circulation pattern and sediment transport restricting deposition to the deeper parts of the seas. It is highly likely that prior to and during the LGM the exchange of water and sediments between the Andaman Sea and Bay of Bengal was completely restricted to the narrow "Preparis South Channel" (Fig. 4.25a), as the "Preparis North Channel" was non-existence because of lower sea level (Fig. 4.25b). After the LGM, major changes occurred in the

supply and deposition of sediments, eustatic sea level and surface circulation patterns in the north-eastern Indian Ocean. These were related to increase in precipitation and discharge by rivers (Goodbred and Kuehl, 2000). Subsequent rise in sea level flooded the continental margin and most of the discharged sediment load possibly got trapped in the inner shelf of Myanmar continental margin. The rise in sea-level might have opened up the broad "Preparis North Channel" and which in turn resulted in strengthening of the surface current in the north-western Andaman Sea and brought in substantial quantity of sediments from the NE Bay of Bengal. We envisage that the observed increase in contribution of the Indo-Burman Range sediments to our core site could have occurred either by removal of already deposited sediments from the western shelf of Myanmar in the NE Bay of Bengal (Fig. 4.25) by the easterly flowing surface currents, or by direct sediment supply from the Indo-Burman Ranges to the core site through the Irrawaddy river system, or by both. This contribution from the Indo-Burman Ranges, however, becomes less pronounced in the sediments deposited in the eastern and southern Andaman Sea (Fig. 4.24). The isotopic compositions of the sediments in the core MD77-169 from the southern Andaman Sea have been interpreted to represent the more radiogenic Sr bearing sediments of the Irrawaddy (Colin et al., 1999). We, therefore, rule out the possibility that the Irrawaddy river system ever carried isotopically non-radiogenic (Sr) sediments derived from the Indo-Burman Ranges into the Andaman Sea. Arguably, the lowering of the sea level during the last glacial period had an important control over the dispersal of sediments in this region.